(0.15 ± 0.12/alveolus) (Fig. 1*D*). Similarly, the number of MN accumulated within the alveolar septa in the high tidal group (0.09 ± 0.01) was significantly higher than that in the control (0.04 ± 0.10, $P < 0.05$) and low tidal groups (0.03 ± 0.05, $P < 0.05$) (Fig. 1*D*).

Expression of ICAM-1, VCAM-1, and P-selectin in lungs evaluated by immunohistochemical staining. Alveolar walls in the lungs of the control and low tidal groups showed faint but positive immunoreactivity for ICAM-1. ICAM-1 expression

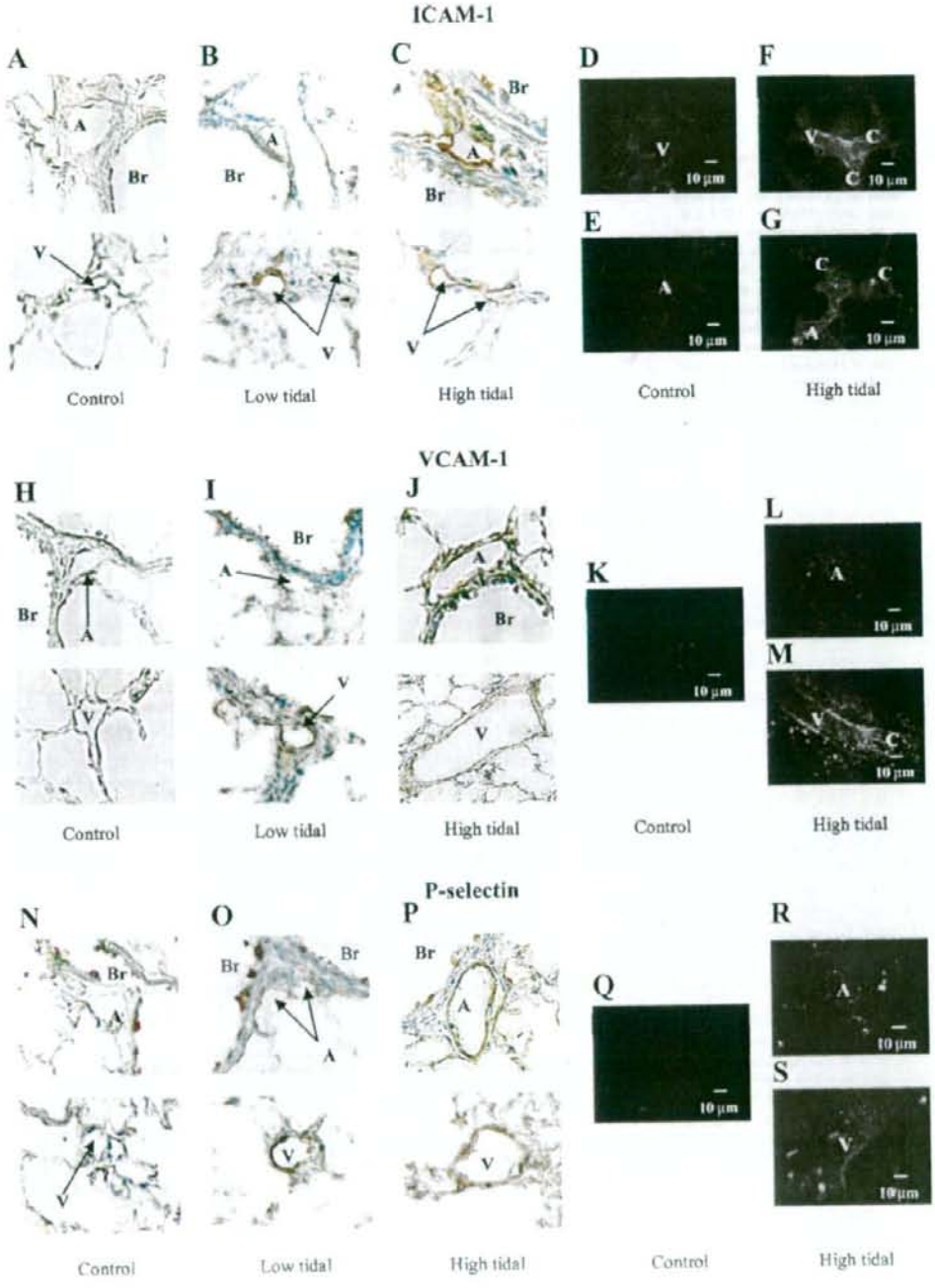

Table 1. *Upregulation of various classes of adhesion molecules in high tidal-ventilated lung*

	ICAM-1	VCAM-1	P-Selectin
Arteriole	++	+	-
Venule	++	++	++
Capillary	++	++	+

++, Strong; +, faint.

was also detected along venules and capillaries, but not along arterioles, in the lungs of the control and low tidal groups (Fig. 2, *A* and *B*). In high tidal volume-ventilated lungs, ICAM-1 expression was appreciably enhanced along the alveolar walls as well as venular and capillary segments. Furthermore, ICAM-1 expression was upregulated and discernible along the arteriolar walls in high tidal volume-ventilated lungs (Fig. 2*C*).

Although neither VCAM-1 nor P-selectin was found to be expressed along the alveolar walls and lumens of any microvessels in the control and low tidal groups, they were sparsely but perceptibly enhanced along arteriolar, venular, and capillary lumens in the high tidal group (Fig. 2, *H–J* and *N–P*).

Expression of ICAM-1, VCAM-1, and P-selectin along microvessel walls evaluated by intravital fluorescence microscopy. In negative control experiments involving the administration of mouse IgG and FITC-labeled anti-mouse IgG antibody, no fluorescence was detectable along microvascular walls in any experimental group. Intravital confocal fluorescence analysis confirmed that ICAM-1 was expressed along venular and capillary walls, but not along arteriolar walls, in the control group (Fig. 2, *D* and *E*). On the other hand, ICAM-1 was significantly upregulated not only along venular and capillary walls, but also along arteriolar walls, during the development of VILI (Fig. 2, *F* and *G*).

VCAM-1 was not detectable along any microvessels in the control group (Fig. 2*K*). VCAM-1 was upregulated in both venular and capillary walls, but not in arteriolar walls, in the high tidal group (Fig. 2, *L* and *M*).

In the control group, P-selectin was not detectable in any microvessels (Fig. 2*Q*). Although P-selectin was appreciably upregulated along venular walls in the high tidal group, P-selectin expression was not evident along arteriolar and capillary walls (Fig. 2, *R* and *S*).

Compared with immunohistochemical study, intravital fluorescence microscopy has some advantages, especially in the identification of microvessels along which a given adhesion molecule is expressed. The intravital microscopic method allows examination of adhesion molecule expression under conditions in which microcirculatory flow is maintained. Therefore, arterioles and venules are easily identified from the difference in their flow directions. However, the sensitivity in detecting the expression of each adhesion molecule is expected to be relatively low with the intravital microscopic method compared with immunohistochemical staining. On the basis of these facts, we classified the degree of expression of each adhesion molecule into two categories: strong and faint enhancement. Strong enhancement was defined as upregulation of the adhesion molecule confirmed by both intravital microscopy and immunohistochemical study, whereas faint enhancement was defined as upregulation detected by immunohistochemical study only (Table 1). According to this classification, ICAM-1 expression was shown to be strongly enhanced along all microvessels, including arterioles, venules, and capillaries in high tidal volume-ventilated lungs. On the other hand, VCAM-1 expression was strongly enhanced along venules and capillaries but faintly enhanced along arterioles in VILI lungs. P-selectin expression in high tidal volume-ventilated lungs was strongly enhanced only in venules but faintly enhanced in both arterioles and capillaries.

Kinetics of PMN in pulmonary microcirculation. There were no significant differences in the vascular diameter including those of precapillary arterioles, postcapillary venules, and capillaries between the control, low tidal, and high tidal groups. The arteriolar diameter analyzed averaged 20.2 ± 3.4 μm in the control group, 20.7 ± 4.1 μm in the low tidal group and 19.9 ± 3.7 μm in the high tidal group. The mean venular diameter was nearly the same as that of arterioles, i.e., 22.4 ± 5.2 μm in the control group, 20.1 ± 3.9 μm in the low tidal group, and 21.8 ± 5.2 μm in the high tidal group, with no difference among the three groups. Addition of MAb against any adhesion molecule exerted little influence on microvascular diameter.

Vmean in arterioles was 0.92 ± 0.36 mm/s in the control group, 1.08 ± 0.75 mm/s in the low tidal group, and 0.93 ± 0.57 mm/s in the high tidal group, corresponding to a wall shear rate of 395, 419, and 394 s^{-1}, respectively. Venular Vmean was 1.03 ± 0.48 mm/s in the control group, 1.12 ± 0.57 mm/s in the low tidal group, and 1.37 ± 0.61 mm/s in the high tidal group, yielding a wall shear rate of 379, 464, and 523 s^{-1}, respectively. The values of Vmean and shear rates in arterioles were not significantly different among the control group, the low tidal group, and the high tidal group. Similarly, both values in venules among three groups were not significantly different. Vmean and wall shear rate were not influenced by the addition of any MAb. Vmean as well as wall shear rates tended to be lower in arterioles than those in venules, but statistically not significant.

We found no PMN adhering firmly to the arteriolar and venular walls under any experimental condition. In the high tidal group, the frequency of rolling PMN was much higher not only in venules (25.4 ± 14.8%), but also in arterioles (34.6 ± 15.2%), than in the control group (venule: 8.1 ± 11.6% vs. VILI, $P < 0.05$, arteriole: 11.8 ± 13.1% vs. High, $P < 0.05$) and in the low tidal group (venule: 5.5 ± 11.1% vs. High, $P < 0.05$, arteriole: 15.5 ± 8.7% vs. High, $P < 0.05$) (Fig. 3*A*). The augmentation of PMN rolling along the venular wall in high tidal volume-ventilated lungs was clearly inhibited by MAb against ICAM-1, VCAM-1, or P-selectin (Fig. 3*A*). Although PMN rolling along the arteriolar wall in the high tidal group was significantly inhibited by either anti-ICAM-1 MAb or anti-VCAM-1 MAb, it was not inhibited by the administration of anti-P-selectin MAb (Fig. 3*A*).

The frequency of PMN entrapped within capillary segments for at least 20 ms (temporal and sustained entrapment) was enhanced in the high tidal group (45.2 ± 10.4%) compared with the control group (25.3 ± 1.4% vs. High, $P < 0.05$) and the low tidal group (17.4 ± 6.1% vs. High, $P < 0.05$). This enhancement was significantly suppressed by anti-ICAM-1 MAb but not by anti-VCAM-1 or anti-P-selectin MAb (Fig. 4*A*). In our experimental systems, the isolated lungs were perfused with the constant flow, and the leukocyte kinetics was measured under steady state and confirmed by confocal laser

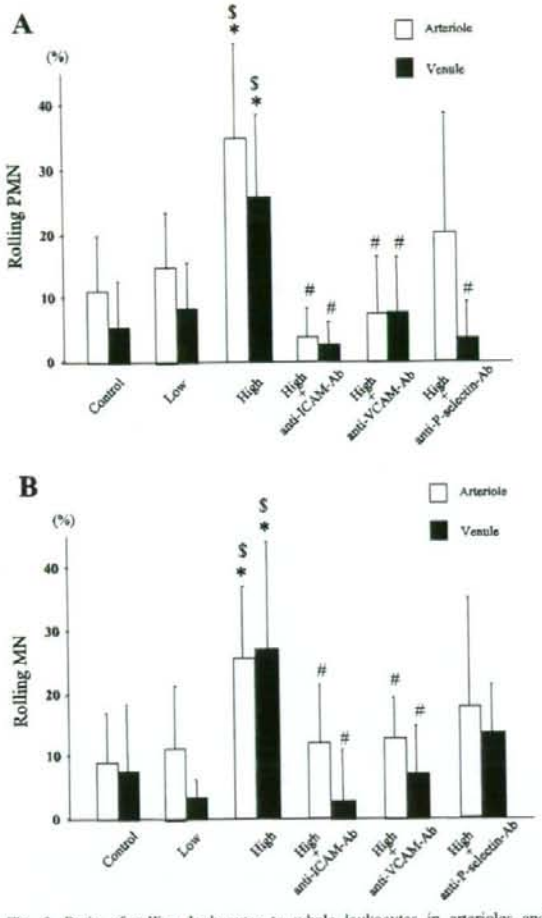

Fig. 3. Ratio of rolling leukocytes to whole leukocytes in arterioles and venules. Control, control lungs; Low, low tidal volume-ventilated lungs without addition of any MAb; High, high tidal volume-ventilated lung without addition of any MAb; Anti-ICAM-Ab, addition of anti-ICAM-1 MAb in high tidal volume-ventilated lung; Anti-VCAM-Ab, addition of anti-VCAM-1 MAb in high tidal volume-ventilated lung; Anti-P-selectin-Ab, addition of anti-P-selectin MAb in high tidal volume-ventilated lung. *A*: relative frequency of rolling PMN in arterioles and venules of high tidal volume-ventilated lung. *B*: relative frequency of rolling MN in arterioles and venules of high tidal volume-ventilated lung. *Significantly higher than value obtained in control lungs; $significantly higher than value obtained in low tidal volume-ventilated lungs; #significantly lower than value in high tidal volume-ventilated lung in the absence of any MAb.

microscopy. Therefore, the capillary switching could not be observed (1).

Kinetics of MN in pulmonary microcirculation. MN did not show firm adhesion to microvessel walls, including arterioles and venules, under any experimental condition. The frequency of rolling MN in venules was significantly higher in the high tidal group (24.7 ± 16.3%) than in both the control (10.0 ± 11.0% vs. High, $P < 0.05$) and low tidal groups (2.6 ± 2.8% vs. High, $P < 0.01$) (Fig. 3*B*). Similarly, rolling MN along the arteriolar wall in the high tidal group (32.4 ± 18.0%) were more evident than in both the control (13.5 ± 14.3% vs. High, $P < 0.05$) and low tidal groups (11.0 ± 10.3% vs. High, $P < 0.05$) (Fig. 3*B*). The augmentation of MN rolling along the venular wall in the high tidal group was significantly inhibited by either anti-ICAM-1 MAb or anti-VCM-1 MAb, but not by anti-P-selectin MAb (Fig. 3*B*). The same tendency was observed for arteriolar MN rolling, as well (Fig. 3*B*).

The number of MN entrapped in capillaries was found to be significantly higher in the high tidal group (47.8 ± 19.3%) than in both the control (27.3 ± 12.2% vs. High, $P < 0.05$) and low tidal groups (24.1 ± 18.3% vs. High, $P < 0.05$). The enhanced entrapment of MN in capillary segments was effectively inhibited by MAb against ICAM-1 or VCAM-1 (Fig. 4*B*).

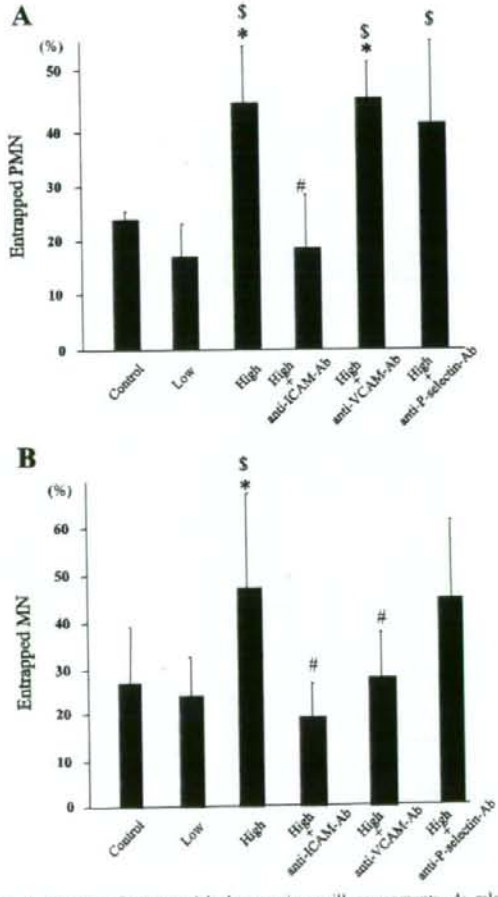

Fig. 4. Number of entrapped leukocytes in capillary segments. *A*: relative frequency of entrapped PMN in capillaries of high tidal volume-ventilated lung. *B*: relative frequency of entrapped MN in capillaries of high tidal volume-ventilated lung. See Fig. 3 legend for bar definitions. *Significantly different from value obtained in control lungs; $significantly higher than value obtained in low tidal volume-ventilated lungs; #significantly lower than value in high tidal volume-ventilated lung in the absence of any MAb.

DISCUSSION

Expression of adhesion molecules in lungs with VILI. The present study demonstrated that ICAM-1 is constitutively expressed along venular and capillary walls, but not along arteriolar walls, in intact rat lungs (Fig. 2). This is consistent with our previous work (18, 22) and also with the work reported by Shen and colleagues (25), who demonstrated constitutive ICAM-1 expression on unstimulated cultured human pulmonary microvascular endothelial cells (HPMEC). Wang and coworkers (33) found that neutrophil adhesion through ICAM-1 induced signaling events leading to cytoskeletal changes only in pulmonary microvascular endothelial cells, the site of neutrophil emigration and edema formation, and not in pulmonary arterial endothelial cells. Nishio et al. (18) reported that P-selectin showed scattered upregulation along arteriolar walls in lungs injured by sustained exposure to a hyperoxic environment, but not along any microvessels, including arterioles, venules, and capillaries in intact rat lungs. Supporting this finding, Shen et al. (25) did not detect significant expression of either P-selectin or VCAM-1 on unstimulated HPMEC, though these two adhesion molecules were markedly upregulated upon stimulation by TNF-α for 4–10 h. Bhattacharya et al. (3) reported that high tidal ventilation upregulated P-selectin on the fresh lung endothelial cells obtained from the rats exposed to high tidal volume ventilation. These findings are highly consistent with those observed in the present study in which neither immunohistochemical study nor intravital fluorescence microscopy detected significant expression of VCAM-1 and P-selectin along any microvessels in control lungs (Fig. 2).

In lungs with VILI, the expression of ICAM-1, VCAM-1, and P-selectin was found to be faintly or strongly enhanced along all the microvessels analyzed (Figs. 2–5 and Table 1). To our knowledge, there has been no authentic study confirming the upregulation of these adhesion molecules along arteriolar segments in the pulmonary microcirculation. We did not obtain evidence of upregulation of ICAM-1 along arteriolar walls in hyperoxia-injured lungs (18) or in bleomycin-induced fibrotic lungs (22) by applying the same method as used for the present analysis. On the basis of these facts, we consider that enhanced expression of ICAM-1, and probably VCAM-1 and P-selectin, along arteriolar walls is a unique event occurring in lungs injured by sustained artificial ventilation. The reason why VILI specifically enhances adhesion molecule expression in pulmonary arterioles, which is not seen in other models of lung injury, is not clear, but we speculate that one of the reasons is the stimuli by VILI is a mechanical stress and stronger than other stimuli such as hyperoxia or endotoxin. Therefore, further study is necessary to elucidate the actual cause of VILI-evoked upregulation of various adhesion molecules along arteriolar walls in the lung.

There is some room for doubt about the significance of endothelial VCAM-1 in modulating PMN kinetics along microvessels in diseased lungs, because of the uncertainties concerning the expression of its counterpart ligand, very late antigen-4 (VLA-4), on the PMN surface. VLA-4 has been considered to be mainly expressed on the mononuclear cell surface. Rieu et al. (21) as well as Lund-Johansen and Terstappen (14) reported that VLA-4 was not detected on the PMN surface, whereas Ibbotson et al. (9) showed that VLA-4 could be mobilized from intracellular granules to the plasma membrane in human blood PMN upon cell activation or during transendothelial migration. In addition, Shang and Issekutz (24) reported that VLA-4 was expressed on the surface of C5a-activated PMN, thus mediating ICAM-1-independent migration of PMN through the vascular endothelium to lung connective tissue. The integrin VLA-9, also expressed on neutrophils, is an alterative receptor for VCAM-1 (30). Although we could not directly measure the levels of VLA-4 and VLA-9 expression on the PMN surface, we believe that the interactions between endothelial VCAM-1 and PMN VLA-4 and VLA-9 are important pathways causing the abnormal microvascular kinetics of leukocytes, including MN and PMN in high tidal volume-ventilated lungs. This is because inhibition of VCAM-1 improved the microvascular rolling of MN and PMN in high tidal volume-ventilated lungs (Fig. 3).

There is no doubt about the importance of endothelial P-selectin in the mediation of abnormal leukocyte kinetics (PMN and MN) in pulmonary microvessels, especially in venules and capillaries, in diseased lungs. Bless et al. (4) demonstrated that, in the cobra venom factor model, P-selectin was upregulated along venular and capillary walls within 1 h, followed by its sustained expression for the next 7 h. Furthermore, P-selectin was confirmed to play a vital role in the development and pathogenesis of various types of lung injury (12, 16, 17). However, to our knowledge, no significant role of enhanced arteriolar P-selectin in evoking lung injury has been conclusively demonstrated. In the present study, we therefore attempted to clarify the importance of P-selectin expressed along arteriolar walls in addition to venular walls and capillary segments in the initial phase of lung injury caused by sustained artificial ventilation.

Importance of adhesion molecules modulating PMN kinetics in high tidal volume-ventilated lungs. Augmented PMN rolling along postcapillary venules in high tidal volume-ventilated lungs was significantly suppressed by MAb against ICAM-1, VCAM-1, or P-selectin (Fig. 3), indicating that these adhesion molecules are equally important for inducing venular PMN rolling in ventilator-associated lung injury. The direct effect of VILI on the adhesion molecule expressions of white blood cells is unclear. Ohta and coworkers (19) reported that in rat lungs receiving high tidal ventilation, the expression of Mac-1 and ICAM-1 on neutrophils and macrophages increased significantly more than in the low tidal ventilation. On the other hand, Choudhury and coworkers (7) showed in an in vivo mouse model of VILI that PMN sequestration in injurious ventilation was markedly inhibited by administration of anti-L-selectin antibody, but not by anti-CD18 antibody, suggesting that this phenomenon is mediated by L-selectin-dependent but CD18-independent mechanisms. Interestingly, however, no rolling PMN qualitatively similar to those seen in systemic venules appeared; i.e., rolling leukocytes in systemic venules frequently show caterpillar-like movement (32), whereas rolling PMN observed in pulmonary venules revealed smooth movement with a significant reduction in velocity compared with that of erythrocytes flowing in the central part of the microvessel. Furthermore, we should emphasize the fact that firm tethering of PMN along venular walls was not observed under any experimental condition in both intact and VILI preparations of our experimental system. These findings are in radical contradiction to the sequential two-step theory of en-

dothelium-leukocyte interaction developed to explain leukocyte rolling and subsequent firm adhesion to vessel walls in the systemic microcirculation (6, 13, 32). Several lines of evidence based on observations in the systemic microcirculation showed that the selectin family such as P-selectin (endothelial surface) and/or L-selectin (leukocyte surface) would initiate cell rolling along microvessels (especially venules) as the first step, leading to firm adhesion mediated by the immunoglobulin superfamily such as ICAM-1 expressed on the microvascular endothelium as the second step (6). Our findings suggest that the second step of firm adhesion of PMN to endothelial cells is lacking or very weak in pulmonary venules, and only the rolling step of PMN plays a role in promoting the venular sequestration of these cells in diseased lungs. A further interesting point is that, besides P-selectin, both ICAM-1 and VCAM-1, which are adhesion molecules inducing firm adhesion between PMN and endothelial cells in systemic venules, act to cause PMN rolling in pulmonary venules.

In arterioles, augmented PMN rolling in high tidal volume-ventilated lungs was appreciably improved by the inhibition of endothelial ICAM-1 or VCAM-1 but not by the inhibition of P-selectin (Fig. 3). Although these findings are somewhat different from those observed for venules, in which all three adhesion molecules contribute equally to PMN rolling, they suggest that rolling in arterioles is as important as that in venules for PMN sequestration into the pulmonary microcirculation in high tidal volume-ventilated lungs. Again, we would like to emphasize the fact that ICAM-1- and VCAM-1-dependent, but P-selectin-independent, arteriolar PMN rolling, which is expected to reflect the initial stage of tissue injury, should be taken as a phenomenon unique to ventilator-associated lung injury.

The importance of various adhesion molecules expressed along capillary segments seems to differ qualitatively from that along venular or arteriolar walls, because we found that only ICAM-1 contributed to the enhanced capillary entrapment of PMN in high tidal volume-ventilated lungs (Fig. 4). The pathological significance of either VCAM-1 or P-selectin expression in abnormal PMN kinetics in capillaries with high tidal volume ventilation is not clear at present. Further study is necessary to demonstrate their exact role. Combining the findings on PMN kinetics observed for arterioles, venules, and capillaries, we can conclude that the contribution of different classes of adhesion molecules to PMN kinetics in the pulmonary microcirculation is vessel type specific (Table 2). Furthermore, besides the cell entrapment in capillary segments, PMN accumulation in the pulmonary microcirculation in ventilator-associated lung injury appears to be preferentially mediated via rolling, but not via firm adhesion, in both arterioles and venules.

Table 2. *Adhesion molecules influencing abnormal leukocyte (PMN or MN) behavior in microvessels in high tidal-ventilated lung*

	Rolling or Capillary Entrapment	
	PMN	MN
Arteriole	ICAM-1 VCAM-1	ICAM-1 VCAM-1
Venule	ICAM-1 VCAM-1	ICAM-1 VCAM-1
Capillary	P-selectin ICAM-1	ICAM-1 VCAM-1

PMN, polymorphonuclear cell; MN, mononuclear cell.

Importance of adhesion molecules modulating MN kinetics in high tidal volume-ventilated lungs. MN, especially lymphocytes, are also expected to be of importance in the pathogenesis of VILI, though there has been no detailed analysis concerning the contribution of MN to VILI. Indeed, we found that the number of MN in BALF harvested from lungs injured by sustained artificial ventilation was greatly increased compared with that in BALF both from control and low tidal volume-ventilated lungs (Fig. 1). Furthermore, the accumulation of MN within the alveolar septa was significantly enhanced in high tidal volume-ventilated lungs (Fig. 1), suggesting that analysis of the microcirculatory kinetics of MN is as pivotal as that of PMN for understanding the entire pathological aspect of VILI. On the basis of this background, we investigated the dynamic behavior of fluorescein-labeled MN in pulmonary microvessels of isolated lungs with high tidal volume ventilation by adding a solution mainly consisting of lymphocytes to the perfusion circuit. Contrary to the findings obtained for PMN, P-selectin had no effect on the behavior of MN in any microvessels in high tidal volume-ventilated lungs (Figs. 3 and 4). Similar to PMN, however, anti-ICAM-1 or anti-VCAM-1 MAb improved the abnormal MN behavior in arterioles and venules (Fig. 3). Differing from PMN, VCAM-1 appeared to significantly enhance MN entrapment in capillaries (Fig. 4). These findings indicate that the relative contribution of endothelial adhesion molecules to the initiation of abnormal leukocyte kinetics in the pulmonary microcirculation differs significantly between PMN and MN, although ICAM-1 is universally important for the kinetics of both cells in any microvessels of lungs with high tidal volume ventilation.

To summarize the findings obtained from lungs with VILI (Tables 1 and 2): the expression of endothelial adhesion molecules differs quantitatively between different microvessels; i.e., ICAM-1 expression is strongly enhanced along all microvascular walls, including arterioles, venules, and capillaries, whereas VCAM-1 is strongly upregulated in venules and capillaries but weakly upregulated in arterioles. P-selectin expression is significantly enhanced along venular walls but weakly enhanced along arteriolar and capillary walls. Consistent with the findings of adhesion molecule expression, the abnormal cell kinetics of both PMN and MN is importantly mediated via an ICAM-1-dependent pathway in all microvessels, suggesting that ICAM-1 inhibition could play a pivotal role as an effective therapeutic strategy in preventing the development of VILI. Furthermore, we would like to stress the fact that ICAM-1- and VCAM-1-dependent arteriolar rolling of PMN and MN appears to function as a specific mechanism for the accumulation of these inflammatory cells in the pulmonary microcirculation in the early stage of VILI.

ACKNOWLEDGMENTS

We are grateful to Drs. T. Aoki, N. Sato, K. Naoki, and Y. Iigo for helpful advice. We also sincerely thank Dr. M. Miyasaka, Osaka University Medical School, Osaka, for generously donating 1A29, and Dr. H. Yagita, Juntendo University, School of Medicine, Tokyo, for generously donating MR106.

REFERENCES

1. **Baumgartner WA Jr, Peterson AJ, Presson RG Jr, Tanabe N, Jaryszak EM, and Wagner WW Jr.** Blood flow switching among pulmonary capillaries is decreased during high hematocrit. *J Appl Physiol* 97: 522–526, 2003.
2. **Belcher JD, Marker PH, Weber JP, Hebbel RP, and Vercellotti GM.** Activated monocytes in sickle cell disease: potential role in the activation of vascular endothelium and vaso-occlusion. *Blood* 96: 2451–2459, 2000.
3. **Bhattacharya S, Sen N, Yiming MT, Patel R, Parthasarathi K, Quadri S, Issekutz AC, and Bhattacharya J.** High tidal volume ventilation induced proinflammatory signaling in rat lung endothelium. *Am J Respir Cell Mol Biol* 28: 218–224, 2003.
4. **Bless NM, Tojo SJ, Kawarai H, Natsume Y, Lentsch AB, Padgaonkar VA, Czermak BJ, Schmal H, Friedl HP, and Ward PA.** Differing patterns of P-selectin expression in lung injury. *Am J Pathol* 153: 1113–1122, 1998.
5. **Brower RG.** Mechanical ventilation in acute lung injury and ARDS. Tidal volume reduction. *Crit Care Clin* 18: 1–13, 2002.
6. **Carlos TM and Harlan JM.** Leukocyte-endothelial adhesion molecules. *Blood* 84: 2068–2101, 1994.
7. **Choudhury S, Wilson MR, Goddard ME, O'Dea KP, and Takata M.** Mechanisms of early pulmonary neutrophil sequestration in ventilator-induced lung injury in mice. *Am J Physiol Lung Cell Mol Physiol* 287: L902–L910, 2004.
8. **Gaehtgens K, Pries AR, and Ley K.** Structural, hemodynamic and rheological characteristics of blood flow in the circulation. In: *Clinical Hemorheology*, edited by Chien S, Dormandy J, Ernst E, and Matrai A. Dordrecht, The Netherlands: Martinus Nijhoff, 1987, p. 97–124.
9. **Ibbotson GC, Doig C, Kaur J, Gill V, Ostrovsky L, Fairhead T, and Kubes P.** Functional α_4-integrin: a newly identified pathway of neutrophil recruitment in critically ill septic patients. *Nat Med* 7: 465–469, 2001.
10. **Imanaka H, Shimaoka M, Matsuura N, Nishimura M, Ohta N, and Kiyono H.** Ventilator-induced lung injury is associated with neutrophil infiltration, macrophage activation, and TGF-β1 mRNA upregulation in rat lungs. *Anesth Analg* 92: 428–436, 2001.
11. **Katayama T, Ikeda Y, Handa M, Tamatani T, Sakamoto S, Ito M, Ishimura Y, and Suematsu M.** Immunoneutralization of glycoprotein Ibα attenuates endotoxin-induced interactions of platelets and leukocytes with rat venular endothelium in vivo. *Circ Res* 86: 1031–1037, 2000.
12. **Kyriakides C, Austen W, Wang Y, Favuzza J, Moore FD, and Hechtman HB.** Endothelial selectin blockade attenuates lung permeability of experimental acid aspiration. *Surgery* 128: 327–331, 2000.
13. **Ley K and Gaehtgens P.** Endothelial, not hemodynamic, differences are responsible for preferential leukocyte rolling in rat mesenteric venules. *Circ Res* 69: 1034–1041, 1991.
14. **Lund-Johansen F and Terstappen WMM.** Differential surface expression of cell adhesion molecules during granulocyte maturation. *J Leukoc Biol* 54: 47–55, 1993.
15. **Matthay MA, Bhattacharya S, Gaver D, Ware LB, Lim LH, Syrkina O, Eyal F, and Hubmayr R.** Ventilator-induced lung injury: in vivo and in vitro mechanisms. *Am J Physiol Lung Cell Mol Physiol* 283: L678–L682, 2002.
16. **Moore TM, Khimenko P, Adkins WK, Miyasaka M, and Taylor AE.** Adhesion molecules contribute to ischemia and reperfusion-induced injury in the isolated rat lung. *J Appl Physiol* 78: 2245–2252, 1995.
17. **Mulligan MS, Polley MJ, Bayer RJ, Nunn MF, Paulson JC, and Ward PA.** Neutrophil-dependent acute lung injury. Requirement for P-selectin (GMP-140). *J Clin Invest* 90: 1600–1607, 1992.
18. **Nishio K, Suzuki Y, Aoki T, Suzuki K, Sato N, Naoki K, Kudo H, Tsumura H, Serizawa H, Morooka S, Ishimura Y, Suematsu M, and Yamaguchi K.** Differential contribution of various adhesion molecules to leukocyte kinetics in pulmonary microvessels of hyperoxia-exposed rat lungs. *Am J Respir Crit Care Med* 157: 599–609, 1998.
19. **Ohta N, Shimaoka M, Imanaka H, Nishimura M, Taenaka N, Kiyono H, and Yoshiya I.** Glucocorticoid suppresses neutrophil activation in ventilator-induced lung injury. *Crit Care Med* 29: 1012–1016, 2001.
20. **Pelegri C, Rogriguez-Palmero M, Morante MP, Comas J, Castell M, and Franch A.** Comparison of four lymphocyte isolation methods applied to rodent T cell subpopulations and B cells. *J Immunol Methods* 187: 265–271, 1995.
21. **Rieu P, Lesavre P, and Halbwachs-Mecarelli L.** Evidence for integrins other than β_2 on polymorphonuclear neutrophils: expression of $\alpha_6\beta_1$ heterodimer. *J Leukoc Biol* 53: 576–582, 1993.
22. **Sato N, Suzuki Y, Nishio N, Suzuki K, Naoki K, Takeshita K, Kudo H, Miyao N, Tsumura H, Serizawa H, Suematsu M, and Yamaguchi K.** Role of ICAM-1 for abnormal leukocyte recruitment in the microcirculation of bleomycin-induced fibrotic lung injury. *Am J Respir Crit Care Med* 161: 1681–1688, 2000.
23. **Schmid-Schonbein GW, Fung YC, and Zweifach BW.** Vascular endothelium-leukocyte interaction. *Circ Res* 36: 173–184, 1975.
24. **Shang XZ and Issekutz AC.** β_2 (CD18) and β_1 (CD29) integrin mechanisms in migration of human polymorphonuclear leukocytes and monocytes through lung fibroblast barriers: sheared and distinct mechanisms. *Immunology* 92: 527–535, 1997.
25. **Shen J, Ham RG, and Karmiol S.** Expression of adhesion molecules in cultured human pulmonary microvascular endothelial cells. *Microvasc Res* 50: 360–372, 1995.
26. **Slutsky AS and Tremblay LN.** Multiple system organ failure. Is mechanical ventilation a contributing factor? *Am J Respir Crit Care Med* 157: 1721–1725, 1998.
27. **Suematsu M, DeLano FA, Poole D, Engler RL, Miyasaka M, Zweifach BW, and Shmid-Schonbein GW.** Spatial and temporal correlation between leukocyte behavior and cell injury in postischemic rat skeletal muscle microcirculation. *Lab Invest* 70: 684–695, 1994.
28. **Takata M, Abe J, Tanaka H, Kitano Y, Doi S, Kohsaka T, and Miyasaka K.** Intraalveolar expression of tumor necrosis factor-α gene during conventional and high-frequency ventilation. *Am J Respir Crit Care Med* 156: 272–279, 1997.
29. **Tamatani T and Miyasaka M.** Identification of monoclonal antibodies reactive with the rat homologue of ICAM-1, and evidence for a differential involvement of ICAM-1 in the adherence of resting versus activated lymphocytes to high endothelial cells. *Int Immunol* 2: 165–171, 1990.
30. **Taooka Y, Chen J, Yednock T, and Sheppard D.** The integrin α9β1 mediates adhesion to activated endothelial cells and transendothelial neutrophil migration through interaction with vascular cell adhesion molecule-1. *J Cell Biol* 145: 413–420, 1999.
31. **Tremblay L, Valenza F, Ribeiro SP, Li J, and Slutsky AS.** Injurious ventilation strategies increase cytokines and c-fos m-RNA expression in an isolated rat lung model. *J Clin Invest* 99: 944–952, 1997.
32. **Von Andrian UH, Chambers JD, McEvoy LM, Bargatze RF, Arfors K, and Butcher EC.** Two-step model of leukocyte-endothelial cell interaction in inflammation: distinct roles for LECAM-1 and the leukocyte β_2 integrins in vivo. *Proc Natl Acad Sci USA* 88: 7538–7542, 1991.
33. **Wang Q, Gordon R, Pfeiffer II, Troy S, and Doerschuk CM.** Lung microvascular and arterial endothelial cells differ in their responses to intercellular adhesion molecule-1 ligation. *Am J Respir Crit Care Med* 166: 872–877, 2002.
34. **Xie X, Raud J, Hedqvist P, and Lindbom L.** In vivo rolling and endothelial selectin binding of mononuclear leukocytes is distinct from that of polymorphonuclear cells. *Eur J Immunol* 27: 2935–2941, 1997.
35. **Yamaguchi K, Nishio K, Sato N, Tsumura H, Ichihara A, Kudo H, Aoki T, Naoki K, Suzuki K, Miyata A, Suzuki Y, and Morooka S.** Leukocyte kinetics in the pulmonary microcirculation: observations using real-time confocal luminescence microscopy coupled with high-speed video analysis. *Lab Invest* 76: 809–822, 1997.
36. **Yamaki K, Lindbom L, Thorlacius H, Hedqvist P, and Raud J.** An approach for studies of mediator-induced leukocyte rolling in the undisturbed microcirculation of the rat mesentery. *Br J Pharmacol* 123: 381–389, 1998.
37. **Yiming MT, Patel R, and Bhattacharya S.** High tidal volume-mediated lung endothelial signaling is leukocyte-dependent. *FASEB J* 16: A408, 2002.

doi:10.1016/j.jmb.2006.08.056 J. Mol. Biol. (2006) 363, 702–712

JMB

Available online at www.sciencedirect.com

ScienceDirect

ELSEVIER

Chain Length-dependent Binding of Fatty Acid Anions to Human Serum Albumin Studied by Site-directed Mutagenesis

Ulrich Kragh-Hansen[1]*, Hiroshi Watanabe[2], Keisuke Nakajou[2] Yasunori Iwao[2] and Masaki Otagiri[2]

[1]*Department of Medical Biochemistry, University of Aarhus, Ole Worms Allé Building 1170 DK-8000 Århus C Denmark*

[2]*Department of Biopharmaceutics Graduate School of Pharmaceutical Sciences Kumamoto University 5-1 Oe-honmachi Kumamoto 862-0973 Japan*

**Corresponding author*

Human serum albumin is the most abundant protein in the circulatory system, and one of its principal functions is to transport fatty acids. Binding of octanoate, decanoate, laurate and myristate was studied by a rate-of-dialysis technique. The primary association constants increased, but not linearly, with chain length. The number of high-affinity sites also increased with chain length; octanoate and decanoate bind to one such site, whereas laurate and myristate most probably bind to two sites. Albumin is composed of three homologous helical domains (I–III), which can be subdivided into two subdomains (A and B). For getting information about the positions of the high-affinity sites we produced 13 recombinant isoforms mutated in four different subdomains. Results obtained with these albumins are in accordance with the following model: octanoate and decanoate bind to a single site in subdomain IIIA, laurate binds to sites in subdomains IIIA and IIIB, whereas myristate binds in subdomains IB and IIIB. The results also showed that primary fatty acid binding is sensitive to amino acid substitutions in other parts of the protein. This is in contrast to the effect of amino acid substitutions of genetic albumin variants (alloalbumins). Usually these substitutions, which are situated at the surface of the protein, have no effect on fatty acid binding. Binding of fatty acid anions to different high-affinity sites and the sensitivity of these sites to amino acid substitutions elsewhere in the protein (and perhaps also to other types of modifications) are important factors that could effect simultaneous binding of other ligands, e.g. in patients treated with albumin-binding drugs.

Keywords: human serum albumin; albumin mutants; fatty acid binding; high-affinity sites; conformational changes

Introduction

Human serum albumin (HSA) is a single-chain protein synthesized in and secreted from liver cells. Normally, it is a simple protein, i.e. it is without prosthetic groups and covalently bound carbohydrate or lipid.[1] Based on X-ray crystallographic analyses of HSA and its recombinant version (rHSA), the polypeptide chain of 585 amino acid residues forms a heart-shaped protein with dimensions 80 Å×80 Å×80 Å and with a thickness of 30 Å.[2,3] The protein has about 67% α-helix but no β-sheet and is composed of three homologous domains (I–III). Each of these has two subdomains (A and B) with distinct helical folding patterns that are connected by flexible loops.[2,3]

HSA is one of the principal compounds of the blood, and, due to its high concentration in plasma (ca 0.6 mM), it is responsible for about 80% of the colloid osmotic pressure of that fluid.[1] In addition, albumin has several other functions. For example, it is an important anti-oxidant, possesses enzymatic properties and serves as a transport and depot protein for numerous compounds.[1,4] Under physiological conditions, one of the primary transport roles of HSA is to carry fatty acids, which are poorly soluble in an aqueous environment, and usually the

Abbreviations used: HSA, human serum albumin; rHSA, recombinant HSA; Site I and II, Sudlow's drug binding sites; Site 1–9, fatty acid binding sites.

E-mail address of the corresponding author: ukh@biokemi.au.dk

protein carries 0.3–1 mol of fatty acid per mol of protein,[5] but this value can raise to 6 after maximum exercise or adrenergic stimulation.[1] Here, we have examined the binding of octanoate, decanoate, laurate and myristate to HSA. Although medium-chain fatty acids normally constitute a minor fraction of the non-esterified fatty acids in plasma, interest in the binding of medium-chain fatty acids exists as the level of these can be greatly elevated in certain disease states, in patients fed intravenous medium chain triacylglycerols and in infants treated for low birth weight.[1] Our results showed principal differences in binding of the four fatty acids to HSA.

In an attempt to examine high-affinity fatty acid binding in more detail we also studied their binding to mutants of rHSA. As a guide to select positions for mutagenesis we used the crystal structures of rHSA complexed with fatty acids. Curry and co-workers have studied the structure of rHSA to which, e.g. decanoate, laurate or myristate was bound and observed binding of eight to ten fatty acid molecules per albumin molecule.[6–8] By contrast, the crystal structure of rHSA–octanoate is still unknown. Other types of experiments, many performed with albumin fragments, have suggested that among the eight to ten sites the high-affinity ones are placed in subdomains IB, IIIA and/or IIIB.[1,9] Therefore, we examined high-affinity binding of the four fatty acids mentioned to R117A and H146A (subdomain IB), Y401A, R410A, Y411F, Y411A, Y411S and the double-residue mutant R410A/Y411A (subdomain IIIA) and K525A (subdomain IIIB), all of which were produced using the yeast species *Pichia pastoris* as the expression system.

The unique ligand binding properties of HSA also include binding of a large number of exogenous compounds such as drugs. High-affinity drug binding usually takes place to Sudlow's Site I or Site II.[10] Site I is pre-formed as a pocket within the core of subdomain IIA and involves the lone tryptophan of the protein (Trp214),[2,3,11] whereas the smaller Site II has been assigned to subdomain IIIA and seems to differ from Site I with respect to shape and polarity.[11] In addition to drugs, fatty acid anions can bind to these two sites. Therefore, we also studied high-affinity binding of octanoate, decanoate, laurate and myristate to Site I and Site II mutants, because in this way we could perhaps get some molecular information about the often observed interplay between albumin-bound fatty acids and drugs.[1,4,12] Thus, in addition to studying fatty acid binding to mutations of, e.g., Arg410 and/or Tyr411, which are components of Site II, we also included the Site I mutants K199A, W214A, R218H and H242Q in the present study.

Results and Discussion

Fatty acid binding to HSA

Binding of octanoate, decanoate, laurate and myristate to HSA was investigated by the rate-of-dialysis technique.[13] This approach was used, because it is well suited to quantify high-affinity ligand binding, and because it is less sensitive to any unbound radiochemical impurities in the batches of radioactively labeled fatty acids than, e.g., equilibrium dialysis.[13] The results obtained with the same total concentrations of the fatty acids and a constant protein concentration are given as Scatchard plots in the insets to Figure 1. From the inset to Figure 1(a) it is seen that octanoate binding takes place to one high-affinity site and to a site with much lower affinity. It is probable that binding experiments with still higher octanoate concentrations can reveal the existence of additional low-affinity sites.[14] From the examples given in the main part of Figure 1(a) it is seen in greater detail how K_1 was estimated; the average value of K_1 (±SD) for 14 determinations performed in triplicate is $2.0(\pm0.1)\times10^6$ M^{-1}. The proposal of only one high-affinity site for octanoate is in accordance with previous findings.[15]

As shown in the inset to Figure 1(b), decanoate binds to more sites, i.e. apparently to one site with a high affinity and to some sites with a low affinity. In this case, K_1 was calculated as $5.1(\pm0.2)\times10^6$ M^{-1} ($n=14$). In 1972, Ashbrook *et al.* published a similar study but based on equilibrium dialysis, and also these authors characterized binding by the stepwise equilibrium method (cf. equation (3)).[16] However, the downward progression of their binding curve is less steep than found in our case, and their K_1 was only 1.03×10^5 M^{-1}. The differences between the results of the two studies can be explained by the fact that Ashbrook *et al.* used a high concentration of chloride ions (116 mM NaCl + 4.9 mM KCl) in their medium, because chloride ions are known to diminish simultaneous binding of medium-chain fatty acids to HSA.[17]

^{13}C NMR spectroscopic studies have revealed differences in binding between decanoate and other fatty acid anions, all with ^{13}C-enriched carboxyl carbon atoms.[14] Thus, chemical shift data showed that the first molecule of octanoate and decanoate either bind differently to the same site or bind to different sites of HSA. Furthermore, differences were found in binding characteristics for decanoate and laurate.

In contrast to binding of octanoate and decanoate, binding of laurate takes place to more than one high-affinity site (Figure 1(c), inset). Several authors have proposed binding to two high-affinity sites, both on the basis of a Scatchard analysis[18,19] and from a stoichiometric approach.[20] Ashbrook *et al.*, using a high chloride ion concentration in the medium, did not agree with that binding model but suggested that laurate binding is best described by a series of decreasing K-values.[21] However, the proposal of two high-affinity sites has been supported by ^1H NMR spectroscopic studies.[22] Still, a K_1-value can be estimated, cf. main part of Figure 1(c), and for laurate it was found to be $3.4(\pm0.2)\times10^7$ M^{-1} ($n=14$). This value is comparable to, or slightly higher than, those previously published.[20,23,24]

K_1 for myristate binding was determined to be $3.6(\pm0.3)\times10^7$ M^{-1} ($n=14$), a value which is similar

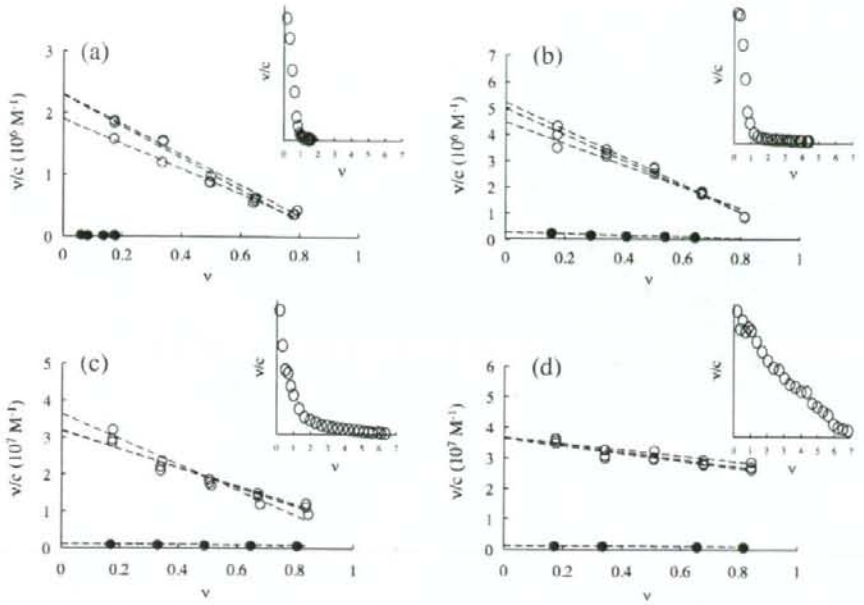

Figure 1. Albumin binding of octanoate (a), decanoate (b), laurate (c) and myristate (d). Main parts show binding to HSA (○) and to the recombinant mutant R410A (●). The symbols represent single determinations. The insets show binding of higher fatty acid concentrations to HSA. These symbols (○) represent average values for five to ten experiments. v stands for the number of mol of fatty acid bound per mol of protein, whereas c is the concentration of unbound fatty acid anion.

to[24,25], or slightly lower than,[23] those previously published. From the inset to Figure 1(d), it is seen that the binding curve for myristate is very different from those characterizing binding of the other three fatty acids with a shorter chain length. The binding curve for myristate is less steep at low v-values, and it has also a much less clear tendency to flatten out. In addition, the flattening out takes place at a higher v-value, namely at $v \sim 2$. These findings indicate, as suggested in the literature,[18,21,25] that the first two molecules of myristate bind to HSA with high affinities, but also that binding of the following molecules takes place with only slightly lower affinities.

The above findings indicate significant differences in the modes of interaction between albumin and the four medium-chain fatty acids. As illustrated by the K_1-values, the binding affinities are dependent on the size of the hydrophobic part of these ligands, a finding that attests to the importance of non-polar forces for binding. However, the increase in the K_1-values is not directly related to chain length: K_1 for laurate is 6.7 times that determined for decanoate, whereas the ratios between K_1 for decanoate/octanoate and myristate/laurate are only 2.6 and 1.1, respectively. Principally the same observation was made by Ashbrook *et al.*, and it can probably be explained by varying degrees of configurational adaptability of the albumin binding sites as the fatty acid increases in length.[21] Tanford has estimated the free energy of association between anionic, aliphatic amphiphiles (carboxylates, sulfates and sulfonates) and native bovine serum albumin.[26] He found that the free energy was linearly dependent on hydrocarbon chain length for ligands having up to eight carbon atoms. By contrast, the free energies of binding were less than expected for amphiphiles of a longer chain length. Tanford explained these findings by assuming size limitation of the binding sites. However, the present observations, and those of Ashbrook *et al.*[21] and Tanford,[26] can perhaps also be explained by a third mechanism, i.e. by fatty acid binding to different regions of the albumin molecule. In any case, the observations show that binding of fatty acids to albumin is not a simple function of chain length.

Fatty acid binding sites of HSA

The most detailed description of fatty acid binding to HSA has been obtained by X-ray diffraction studies of recombinant HSA co-crystallized with specific fatty acids.[6-8] Unfortunately, these investigations did not include binding studies with octanoate. Figure 2(a) shows HSA complexed with decanoate as well as the subdivision of the protein into domains (I – III) and subdomains (A and B). By using a large fatty acid to protein molar ratio it was possible to identify ten binding sites for decanoate (number 1–9 plus 6'). Different types of locations were found, namely sites within subdomains (1, 4 and 7), sites involving residues from more than one subdomain (2, 3, 5, 6 and 6'), and sites placed

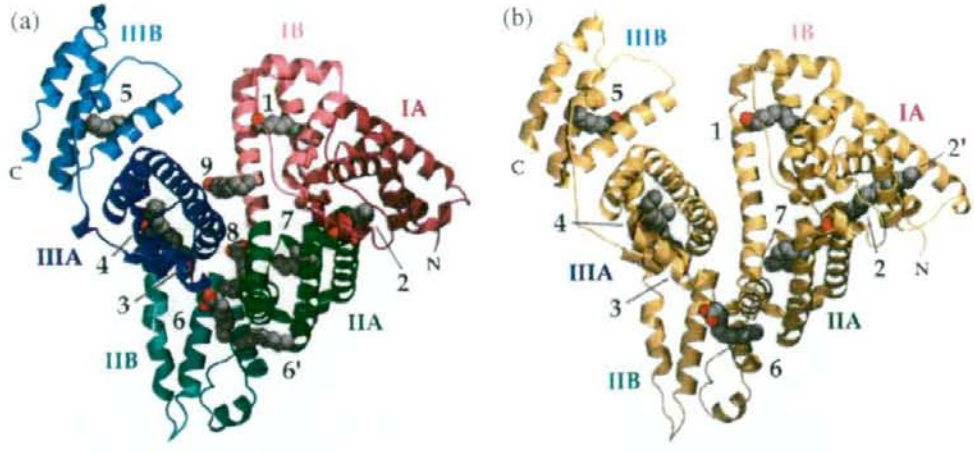

Figure 2. Crystal structure of rHSA complexed with decanoate (a) or laurate (b). The structures reveal ten decanoate binding sites and eight laurate binding sites. The numbering of the sites is taken from Bhattacharya *et al.*[8] The fatty acid anions are depicted in space-filling representation; oxygen atoms and carbon atoms are colored red and grey, respectively. The subdivision of rHSA (and HSA) into domains (I–III) and subdomains (A and B) is indicated. N and C represent the N terminus and C terminus, respectively. The illustrations were made with Molscript on the basis of the atomic coordinates 1e7e (a) and 1e7f (b) available at the RCSB Protein Data Bank.

between subdomains (8 and 9). Of these sites, Sites 6 and 6'are situated on the surface of HSA. Only eight sites were detected for laurate (**Figure 2**(b)) and myristate (not shown), namely Sites 1–7 with the same locations as found for decanoate and a new site (2') placed in subdomain IA. In the following, the site numbering of **Figure 2** will be used. Although the studies referred to[6–8] are a great step forward in our understanding of fatty acid binding to HSA, they are not able to distinguish high-affinity sites from sites with a lower affinity. However, a hint can be found in the case of myristate binding, because only Sites 1–5 were detected using a lower fatty acid to protein molar ratio.[6]

In vivo, albumin is a complex molecule carrying out its functions in aqueous solutions. Therefore, for getting a more complete understanding of the proteins ability to, for example, interact with aliphatic fatty acids it is necessary to perform supplementary studies with albumin in solution. For that purpose, NMR spectroscopy would be useful, but the high molecular mass and helical content of HSA is still a problem to that kind of investigation. Here, we have attempted to throw light on the fatty acid binding properties of HSA by site-directed mutagenesis. When selecting positions for mutagenesis we used the X-ray structures described by Bhattacharya *et al.* (**Figure 2**) as a guide.[8] For mutagenesis we chose ten important residues in the fatty acid binding sites 1, 4, 5 and 7, and the mutated residues are shown in greater detail in **Figure 3**.

Recombinant HSA mutants

The 12 single-residue mutants, the single double-residue mutant and wild-type rHSA were produced using a yeast expression system. Before freeze-drying, all the isolated proteins were treated with charcoal and dialyzed extensively against deionized water for removing any hydrophobic and hydrophilic ligands, respectively. All the albumins were analyzed by far-UV and near-UV CD spectroscopy, and we observed no differences between the spectra for commercial HSA, wild-type rHSA and the mutants. The spectra for most of the proteins have been presented before,[27–29] but the mutants R117A, H146A and Y401A were studied as a part of the present work (not shown). Likewise, the light absorbance spectra (250–350 nm) of all the albumins were comparable (not shown). Thus, the mutations have probably not caused major differences in albumins secondary or tertiary structures.

Fatty acid binding to rHSA mutants

Earlier studies have shown competitive binding of octanoate and diazepam to a common high-affinity site in HSA.[15] Very recently, crystallographic analyses revealed the existence of only one binding site for diazepam, namely a site placed in subdomain IIIA, where the drug interacts with the hydroxyl group of Tyr411 and some hydrophobic residues.[11] Therefore, high-affinity binding of octanoate most probably also takes place in that subdomain, e.g. in Site 3 or 4 reported for binding of fatty acids of a longer chain length (**Figure 3**(c)). Such an assignment is supported by the observations done in the present study with mutants. **Figure 4**(a) shows that mutating Arg410 and/or Tyr411 to alanine decreases K_1 to values that are ≤2% of the original value. These findings can be explained by elimination of a salt-bridge between Arg410 and/or a hydrogen bond between Tyr411 and the carboxylate

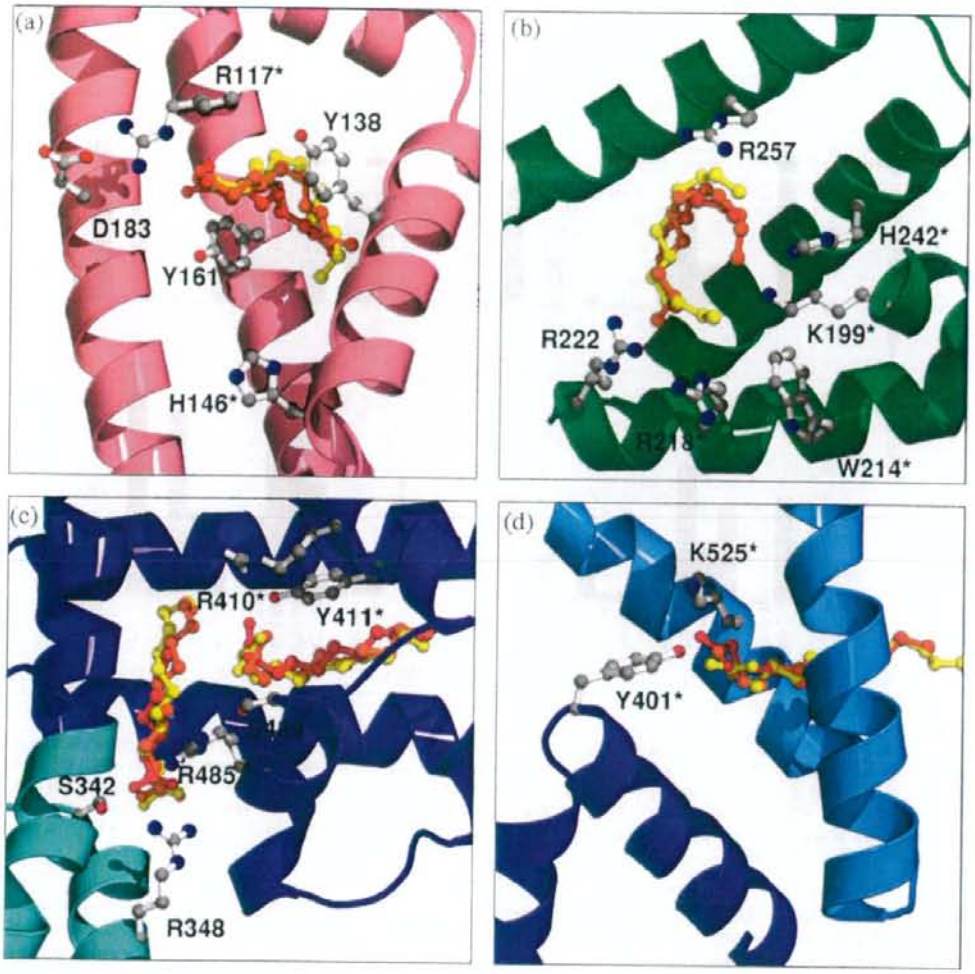

Figure 3. Fatty acid binding to Site 1 in subdomain IB (a), to Site 7 in subdomain IIA (b), to Sites 3 and 4 in subdomains IIB and IIIA (c), and to Site 5 in subdomains IIIA and IIIB (d). The fatty acids are decanoate (red), laurate (orange), and myristate (yellow). The color code for domains and subdomains is the same as that used in **Figure 2**(a). The residues mutated in this work are marked with an asterix. The illustrations were made with Molscript on the basis of the atomic coordinates 1e7e (decanoate), 1e7f (laurate), and 1e7g (myristate) available at the RCSB Protein Data Bank.

group of the fatty acid,[8] suggesting binding of octanoate to Site 4 (**Figure 3**(c)). It is widely accepted that the site is adaptable and can undergo ligand-induced alterations. However, substituting Tyr411 with its OH-group to which octanoate can establish a hydrogen bond with serine, which also possesses an OH-group, greatly diminishes binding affinity (**Figure 4**(a)). Finally, mutating Tyr411 to the hydrophobic phenylalanine has a less dramatic effect on binding.

Surprisingly, mutations in other subdomains of rHSA also decrease K_1 for octanoate binding. **Figure 4**(a) shows that mutations in fatty acid Site 1 (R117A, H146A), Site 7 (K199A, W214A, R218H, H242Q) and Site 5 (Y401A, K525A) also diminish primary octanoate binding. However, taken as small groups of mutations, as indicated in **Figure 4**, octanoate binding is mostly affected by the mutations in Site 4. The effects of mutating residues in Sites 1, 5 and 7 are probably not due to abolished octanoate binding to a secondary site(s), because secondary binding only contributes very little to octanoate binding (cf. **Figure 1**(a), inset). Rather, they are caused by minor, but apparently widespread, conformational changes in the albumin structure. These conformational changes could not be detected by using CD or light absorbance spectroscopy. However, albumin in solution is not a static structure but a molecule changing between different conformational states. The conformational changes involve both small-amplitude fluctuations and large-amplitude fluctuations ("breathing"), and the latter type of changes

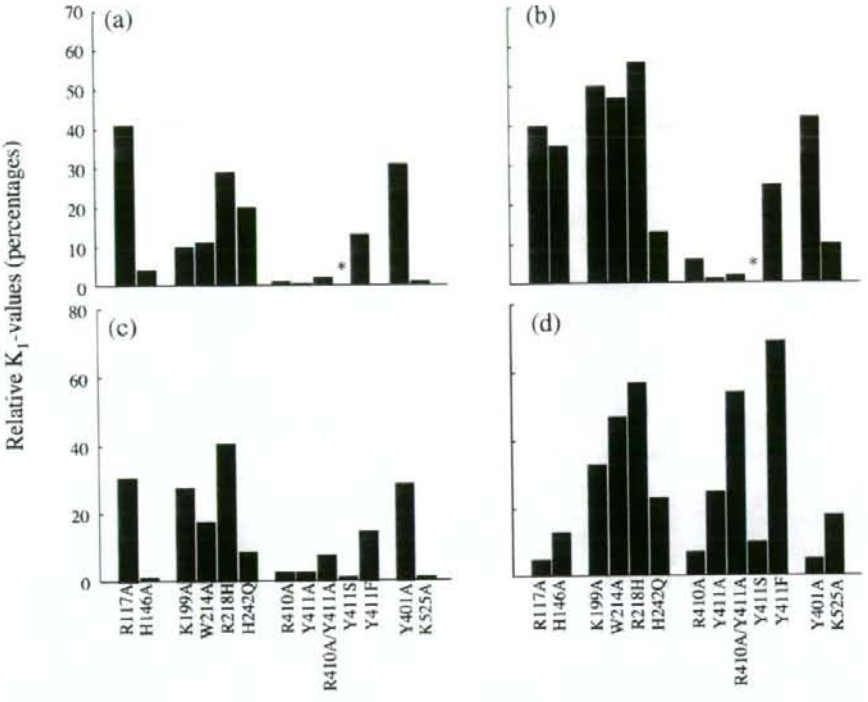

Figure 4. Primary binding of octanoate (a), decanoate (b), laurate (c) and myristate (d) to rHSA mutants. The results are given as K_1-values for the mutants relative to the K_1-values determined for normal albumin. * The relative K_1-value is less than 0.5%. The K_1-values were determined as illustrated in Figure 1, which shows the results for R410A. The Scatchard plots of the binding of each fatty acid to wild-type rHSA and to the remaining mutants are given in Supplementary Data. From Supplementary Data it can be seen that fatty acid binding to wild-type rHSA and HSA are comparable.

can involve relatively large parts of the protein (reviewed by Kragh-Hansen[12]). Thus, even though the two spectroscopic methods could not register any mutation-induced conformational changes, they could still be the explanation for the observed cases of diminished high-affinity binding of octanoate. To our knowledge, these results are the first reported examples of mutation-induced conformational changes affecting ligand binding to other subdomains than the one housing the mutation. However, such effects have previously been observed in the case of ligand-induced conformational changes.[12,30] A recent example is that ligand binding to a sub-site of Site I in subdomain IIA mutually affects binding of diazepam and ibuprofen in subdomain IIIA.[31]

The effects of the mutations on primary decanoate binding were principally the same as those observed for octanoate binding (Figure 4(b)), showing why also decanoate most probably binds with high affinity to Site 4 (Figure 3(c)). Thus, the amino acid substitutions R410A, Y411A, Y411S and the double mutant R410A/Y411A all decreased K_1 to less than 6% of the value determined for normal albumin. In this case as well, mutating Tyr411 to a phenylalanine resulted in a less pronounced decrease of K_1. The other mutations also diminished decanoate binding, although generally to a less pronounced extent than when mutating Arg410 and/or Tyr411. Usually, the diminishing effects on decanoate binding were smaller than those observed for octanoate binding. Because hydrophobic interactions are more important for decanoate binding than for octanoate binding, this finding indicates that formation of hydrophobic interactions are less dependent of the detailed protein structure than, e.g., establishing salt-bridges and hydrogen bonds.

Bhattacharya *et al.*[8] have proposed that Site 7 in subdomain IIA (Figure 3(b)) may be a primary site for shorter-chain fatty acids such as octanoate and decanoate. However, such a proposal is not supported by competition experiments[15] or by the present experimental findings (Figure 4(a) and (b)) which, as argued above, point to Site 4 as the high-affinity site for these fatty acid anions.

Taken as groups of mutations, the mutations in position 410 and 411 have the greatest impact on laurate binding (Figure 4(c)) proposing that also this fatty acid binds with a high affinity to Site 4 (Figure 3(c)). Even though hydrophobic interactions between laurate and HSA must be stronger than those between decanoate and HSA, the effects of the

remaining mutations on laurate binding are more pronounced than the corresponding effects on decanoate binding. This difference is most likely due to the existence of two and not just one high-affinity binding site for laurate. As can be seen from Figure 2, the different effect of the mutations is not caused by an increase in the total number of binding sites for laurate.

Different types of studies with intact albumin and with fragments thereof have proposed the existence of two high-affinity binding sites for long-chain fatty acids such as palmitate and oleate.[7] These sites are probably identical to Sites 1 and 5,[7] with Site 5 having the highest affinity.[7,32] Therefore, even though the two mutations in the two sites have very similar effects on laurate binding (Figure 4(c)), it is tempting to suggest that Site 5 is the additional high-affinity binding site for laurate.

The impacts of the five mutations in position 410 and 411 on myristate binding are principally the same as those observed for the three fatty acid anions of a shorter chain length (Figure 4(d)). However, in the case of myristate the effects are much less pronounced; this is observed especially for Y411F and the double-residue mutant. In addition, the mutations in Site I (K199A, W214A, R218H and H242Q) have only moderate effects on binding. In contrast, all the rHSAs with amino acid substitutions in Site 1 or Site 5 have a greatly diminished affinity for myristate, indicating that the two high-affinity sites for myristate are placed in these sites. Again, Site 5 could represent the highest-affinity binding site. This proposal implies that Site 4 has been "degraded" to a secondary site. As apparent from the following discussion, binding of long-chain fatty acids (e.g. palmitate and oleate) seems to take place according to a similar binding scheme. Thus, high-affinity binding of myristate takes place like fatty acids of a longer chain length and not like laurate and other fatty acids of a shorter chain length.

Kragh-Hansen[12] has proposed, on the basis of ligand competition experiments, an albumin binding model in which the two high-affinity sites for long-chain fatty acids are placed in other regions of the protein than the one binding, e.g., octanoate with high affinity. Using CD spectroscopy, Sjödin registered only a small displacing effect of oleate on HSA-bound diazepam and proposed that the displacement occurred primarily through an allosteric mechanism rather than through direct competition between the two ligands.[33] Cunningham *et al.*[34] found by using an ultrafiltration technique that L-tryptophan binding, taking place to the same site as diazepam,[15] was more decreased by the presence of low concentrations of laurate than by equimolar amounts of palmitate or oleate, even though the latter are bound with much higher affinities. Actually, a marked inhibition of L-tryptophan binding by palmitate and oleate only occurred when their molar ratios to albumin were increased to 2 or above. The binding model is also supported by other types of studies. For example, Koh and Means[35] observed that the esterase-like activity of HSA, which is due to Arg410 and Tyr411,[27] is effectively inhibited by medium-chain fatty acids up to decanoate but not by longer-chain fatty acids.

Very recently, Simard *et al.*[32] investigated the binding of ^{13}C-labeled palmitate and oleate to rHSA and to two mutants thereof by X-ray crystallography and ^{13}C NMR spectroscopy and proposed fatty acid binding to three sites of a high affinity. At a 1:1 molar ratio of fatty acid to albumin two NMR peaks (181.5 and 181.8 ppm) were observed, and a third peak (182.2 ppm) appeared at a 2:1 molar ratio. At higher ratios more peaks appeared. When mutating Lys525 to alanine, one of the first two peaks, the most intense one (181.8 ppm), disappeared or diminished very much, proposing that Site 5 is a high-affinity binding site. The authors also produced a recombinant domain III fragment (residues 382–585), and fatty acid binding to that peptide produced two of the three peaks (181.8 and 182.2 ppm) but not the initial one at 181.5 ppm, suggesting that a high-affinity site is placed N-terminally to domain III. Finally, when mutating both Arg410 and Tyr411 in the intact protein to alanine, the third peak (182.2 ppm), only observed at a molar ratio of 2:1 or higher, disappeared. These results are in full accordance with a binding model proposing Sites 1 and 5 as high-affinity sites and Site 4 as a secondary one, i.e. a binding model similar to that proposed for myristate binding. Simard *et al.*[36] have just expanded their studies on palmitate binding to include drug-competition analyses. The results of these extensive investigations support the binding model except for the assignment of a high-affinity binding site to Site 1 (represented by the peak at 181.5 ppm). From experiments with the R117A mutant and displacement studies with hemin and phenylbutazone the authors suggested that Site 2 and not Site 1 is a high-affinity site. From the present work we cannot exclude that also one of the two high-affinity sites for myristate binding is placed in Site 2 instead of in Site 1, because we have not yet produced mutants in Site 2.

Under normal physiological conditions, albumin carries 0.3–1 mol of fatty acids per mol of protein.[5] At such molar ratios, the fatty acids mainly bind to their respective high-affinity sites. Therefore, it is of physiological, pharmaceutical and pharmacological importance to have some knowledge about the location of these sites, because such knowledge can be useful when predicting potential ligand interactions. For example, our results showed that high-affinity binding of long-chain fatty acids, but not high-affinity binding of octanoate and decanoate, could take place in Site 1 to which also heme binds with a high affinity.[30] Furthermore, in contrast to high-affinity binding of long-chain fatty acids high-affinity binding of octanoate and decanoate takes place to Site 4 and thereby will compete with high-affinity binding of drugs like

diazepam, ibuprofen, diflunisal, halothane and propofol.[11]

Crystallographic analyses of fatty acid–albumin complexes were not able to determine the locations of the carboxylate head-groups and the methyl ends of fatty acids bound in Site 7, while their orientation in that site still is unknown (**Figure 3**(b)).[8] Unfortunately, the present work with recombinant mutants is not able to solve that problem, because binding to Site 7 is low-affinity binding, which does not contribute much to total binding at the molar ratios used here.

Fatty acid binding to natural mutants of HSA

We were surprised to see, that all the recombinant mutations decreased primary fatty acid binding (**Figure 4**); no example of unmodified or increased binding was found. Does this mean that fatty acid binding to albumin is so sensitive that all mutations will affect binding? In an attempt to throw some light on that question we have collected qualitative information for laurate binding, as an example, to genetic variants of HSA. As seen from **Figure 5**, 11 of 13 single-residue mutations had no or only a very small effect on binding, whereas one increased binding and one decreased binding. Thus, it is not obligatory that albumin mutations affect fatty acid binding.

Genetic variants of HSA (alloalbumins) are usually found by electrophoresis under non-denaturing conditions. This implies that the substitutions are located on the surface of the protein molecule and are exposed to the solvent. Therefore, the importance of mutations for fatty acid binding could be so that most of the mutations at albumins surface do not effect binding (**Figure 5**), whereas mutations in the inner parts of the protein, e.g. in binding sites, usually affect binding (**Figure 4**).

Concluding remarks

The K_1-value for binding of octanoate, decanoate, laurate and myristate increases with the chain length of the fatty acid, reflecting the importance of hydrophobic effects for binding. Furthermore, the number of high-affinity binding sites and their location in the albumin molecule most probably also depend on the chain length. Thus, octanoate and decanoate bind to Site 4. By contrast, both laurate and myristate seem to bind to two high-affinity sites, namely Sites 4 and 5 and Sites 1 and 5, respectively (**Figures 2 and 3**). The results obtained with the recombinant mutants and with genetic variants show that fatty acid binding is influenced by amino acid substitutions in the interior of the protein but much less so by mutations of superficially placed amino acid residues.

Binding of fatty acid anions to different high-affinity sites, and the sensitivity of the sites to amino acid substitutions elsewhere in the protein (and perhaps also to other types of modifications) are important factors in cases of simultaneous binding of other ligands. These circumstances have to be taken into account, e.g., when patients are treated with albumin-binding drugs.

In the present work, most of the focus has been on K_1-values. This was done for making interpretations somewhat less complicated. Furthermore, under physiological conditions HSA only carries one mol, or less, of fatty acid anion per mol of protein.

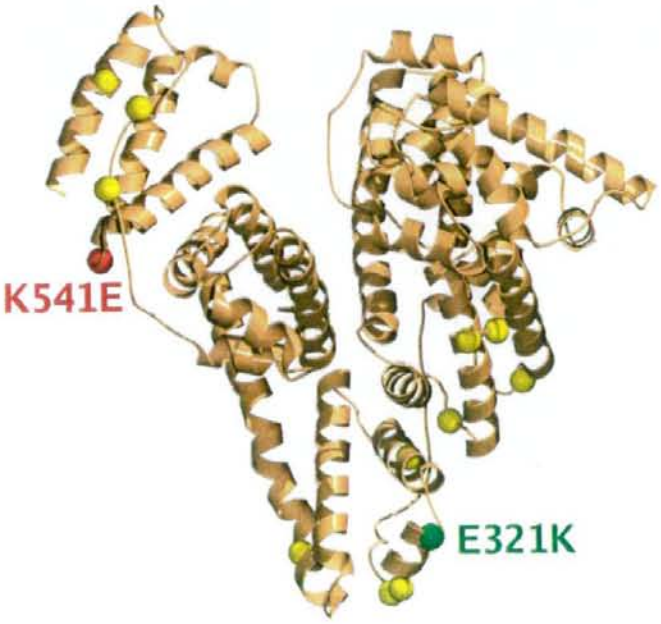

Figure 5. Laurate binding to natural mutants of HSA. Mutation of the residue in green (E321K) and of the one in red (K541E) results in increased and decreased fatty acid binding, respectively. Residues in yellow indicate that substitution of these amino acids does not affect binding much or not at all; the mutations are K225N, K240E, D269G, K276N, K313N, D314V, E333K, K372E, E501K, E505K and K573E. The information is from published[37,38] and unpublished (D314V) observations. The illustration was made with Molscript on the basis of the atomic coordinates 1ao6 available at the RCSB Protein Data Bank.

Materials and Methods

Materials

HSA (A-1887, >96% pure and essentially fatty acid free (less than 0.01 mol/mol albumin, according to the manufacturer)) was obtained from Sigma Chemical Co. (St. Louis, MO, USA). The DNA techniques for producing wild-type rHSA and mutants thereof, using the yeast species *P. pastoris* (strain GS115) as an expression system, have been published.[27,28] The mutagenic primers used for the mutants R410A, Y411A, Y411S, Y411F and for the double-residue mutant R410A/Y411A have been presented,[27] and those used for the single-residue mutants K199A, W214A, R218H and H242Q have been published.[28] Additional mutagenic primers used (underlined letters indicate mismatches) were 5′-CCCCCGATTGGTGGCACCAGAGGTTGATG-3′ for R117A, 5′-GCCAGAAGAGCTCCTTACTTTTATGCCC-3′ for H146A, 5′-GCTTGGAGAGGCCAAATTCCAGAATGCGC-3′ for Y401A and 5′-GACAAATCAAGGCACAAACTGCAC-3′ for K525A. In all cases, the DNA sequence of the entire albumin coding region was verified as described.[27,28] Secreted albumin was isolated from the growth medium and purified as usually done.[27,28] For removing any hydrophobic ligands, the albumins were treated with charcoal at pH 3 as described by Chen,[39] deionized, freeze-dried and then stored at –20 °C until use. The recombinant albumins (treated with dithiothreitol) exhibited a single band on SDS/PAGE, and they all migrated to the same position as HSA. Density analysis of protein bands stained with Coomassie Brilliant Blue showed that the purity of the recombinant albumins was better than 97%. The molecular masses of all the albumins were taken to be 67 kDa.

Octanoic acid (sodium salt) was from Merck (Hohenbrunn, Germany), *n*-decanoic acid was from Sigma, whereas lauric acid and myristic acid were from Fluka Chemika (Buchs, Switzerland). [1-^{14}C]Octanoic acid (53 Ci/mol) and [1-^{14}C]decanoic acid (55 Ci/mol) were from American Radiolabeled Chemicals Inc. (St. Louis, MO, USA), whereas [1-^{14}C]lauric acid (57 Ci/mol) and [9,10(*n*)-^{3}H]myristic acid (54 Ci/mmol) were from Amersham Life Science (Little Chalfont, Buckinghamshire, UK). Other chemicals were also of the best grades commercially available, and all solutions were prepared in doubly deionised water.

Intrinsic CD spectra

Far-UV intrinsic spectra were recorded from 200 to 250 nm using a protein concentration of 1.5 μM in 66 mM sodium phosphate buffer (pH 7.4, 25 °C). Near-UV spectra were obtained from 250 to 350 nm at a protein concentration of 15 μM in the same buffer. All measurements were made with a Jasco J-720 type spectropolarimeter (Tokyo, Japan).

Spectrophotometry

The light absorbance spectra of HSA, rHSA and the mutants (20 μM) dissolved in 66 mM sodium phosphate buffer (pH 7.4) at room temperature were recorded from 250 nm to 350 nm using 1 cm quartz cuvettes and a Shimadzu UV-160A Spectrophotometer (Kyoto, Japan).

Fatty acid binding

Buffered solutions of the fatty acid anions, with or without a small fraction radiolabeled, were prepared; some of the solutions were with albumin. The medium was in all cases 66 mM sodium phosphate (pH 7.4) with 10 mg gentamicin sulfate added per liter at 25 °C. Control experiments revealed that the antibiotic did not interfere with binding. The albumin concentration (30 μM) was determined by dissolving a weighted amount of the protein in the desired volume of buffer and checking spectrophotometrically at 279 nm using the absorbance at 1 mg/ml of 0.531.[1] When studying ligand binding to HSA, the total fatty acid concentrations varied from 5 μM to 210 μM. The binding experiments including the recombinant proteins were carried out with lower total ligand concentrations, namely 5–25 μM.

Binding was quantified by the kinetic dialysis technique described.[13] In short, two types of experiments were performed. For the first type, buffered solutions of 25 μM fatty acid anion, with or without radiolabeled traces, were made. At time zero, 1.0 ml samples of the former and latter type of solutions were pipetted into left and right compartments, respectively, of 2.4 ml Plexiglas cells. Each cell was divided into two equal compartments by a cellulose membrane cut from dialysis tubing (Union Carbide Corp., Chicago, IL, USA). After closure, the filled cells were rotated in a cabinet having a constant temperature of 25 °C. After 5, 10, 15, 20, 25 or 30 min the half-cells were emptied, and 750 μl portions from the left and right compartments were used for liquid-scintillation counting in a Packard Tri-Carb spectrometer.

In the second type of experiments, solutions of different concentrations of fatty acid were prepared with or without radiolabeled fatty acid included. However, these solutions also contained a constant quantity of albumin. At time zero, 1.0 ml samples of the former and latter type of solutions were pipetted into the left and right compartments, respectively, of the dialysis cells. These cells were allowed to rotate in the cabinet for a known time of approximately 3 h (octanoate and decanoate) or 19 h (laurate and myristate). After the half-cells had been emptied, aliquots of 750 μl were taken for liquid-scintillation counting. Because the stock solutions of decanoate, laurate and myristate for both types of experiments were prepared in 4 mM NaOH, the pH of the final solutions was checked at room temperature.

Calculations

In both types of experiments, the time of dialysis was insufficient to establish equilibrium with respect to the radioactive label. Therefore, it is possible to calculate, from the experiments performed without protein, a rate constant, k, for net transfer of unbound fatty acid anion through the dialysis membrane from the following relationship:[13]

$$\ln\left[\frac{Q_l - Q_r}{Q_l + Q_r}\right] = -k \times t \qquad (1)$$

The terms Q_l and Q_r stand for radioactivity in the samples taken from the left and right compartments, respectively, after dialysis for t min. Now, knowing k for unbound ligand, it is possible to determine the concentration of

unbound fatty acid anion, c, in the albumin-containing solutions:[13]

$$\ln\left[\frac{Q_l - Q_r}{Q_l + Q_r}\right] = -k \times t \times \frac{c}{C} \quad (2)$$

In equation (2), C denotes the known concentration of total ligand. Performing experiments with different concentrations of total ligand gives connected values of c and ν; the latter parameter is the number of mol of fatty acid anion bound per mol of protein.

Applying the following equation to the different sets of binding data, ν and c, allows a calculation of stoichiometric association constants, i.e. K_1, K_2,..., K_N:

$$\nu = \frac{K_1 c + 2K_1K_2c^2 + \ldots + NK_1K_2\cdots K_N c^N}{1 + K_1 c + K_1K_2c^2 + \ldots + K_1K_2\cdots K_N c^N} \quad (3)$$

The term N represents the maximum number of ligand molecules that can be bound per albumin molecule.

An estimate of the first stoichiometric constant, K_1, can be obtained by a simple graphical approach. Dividing equation (3) by c leads to:

$$\frac{\nu}{c} = \frac{K_1 + 2K_1K_2c + \ldots + NK_1K_2\cdots K_N c^{N-1}}{1 + K_1 c + K_1K_2c^2 + \ldots + K_1K_2\cdots K_N c^N} \quad (4)$$

From equation (4) it is seen, that if $c \to 0$ (or $\nu \to 0$) then $\nu/c \to K_1$. In practice, the experimental data are plotted as a Scatchard plot, ν/c *versus* ν, and K_1 is obtained by extrapolation of ν to 0.[13]

Calculations of rate constants, k, and binding constants, K_1, were performed by an iterative procedure with the Sigma Plot software from Jandel Scientific, which enables linear regression with confidence intervals.

Acknowledgements

We thank Dr Anders O. Pedersen for help with the experimental work and Dr Morten Kjeldgaard for help in making the molecular illustrations. This work was supported, in part, by Fonden af 1870 and by Grants-in-Aid for Scientific Research from the Ministry of Education, Science, Sports and Culture of Japan (14370759).

Supplementary Data

Supplementary data associated with this article can be found, in the online version, at doi:10.1016/j.jmb.2006.08.056

References

1. Peters, T., Jr (1996). All About Albumin: Biochemistry, Genetics, and Medical Applications. Academic Press, San Diego.
2. He, X. M. & Carter, D. C. (1992). Atomic structure and chemistry of human serum albumin. *Nature*, **358**, 209–215.
3. Sugio, S., Kashima, A., Mochizuki, S., Noda, M. & Kobayashi, K. (1999). Crystal structure of human serum albumin at 2.5 Å resolution. *Protein Eng.* **12**, 439–446.
4. Kragh-Hansen, U., Chuang, V. T. G. & Otagiri, M. (2002). Practical aspects of the ligand-binding and enzymatic properties of human serum albumin. *Biol. Pharm. Bull.* **25**, 695–704.
5. Spector, A. A. (1986). Structure and lipid binding properties of serum albumin. *Methods Enzymol.* **128**, 320–339.
6. Curry, S., Mandelkow, H., Brick, P. & Franks, N. (1998). Crystal structure of human serum albumin complexed with fatty acid reveals an asymmetric distribution of binding sites. *Nature Struct. Biol.* **5**, 827–835.
7. Curry, S., Brick, P. & Franks, N. P. (1999). Fatty acid binding to human serum albumin: new insights from crystallographic studies. *Biochim. Biophys. Acta*, **1441**, 131–140.
8. Bhattacharya, A. A., Grüne, T. & Curry, S. (2000). Crystallographic analysis reveals common modes of binding of medium and long-chain fatty acids to human serum albumin. *J. Mol. Biol.* **303**, 721–732.
9. Hamilton, J. A., Era, S., Bhamidipati, S. P. & Reed, R. G. (1991). Locations of the three primary binding sites for long-chain fatty acids on bovine serum albumin. *Proc. Natl Acad. Sci. USA*, **88**, 2051–2054.
10. Sudlow, G., Birkett, D. J. & Wade, D. N. (1975). The characterization of two specific drug binding sites on human serum albumin. *Mol. Pharmacol.* **11**, 824–832.
11. Ghuman, J., Zunszain, P. A., Petitpas, I., Bhattacharya, A. A., Otagiri, M. & Curry, S. (2005). Structural basis of the drug-binding specificity of human serum albumin. *J. Mol. Biol.* **353**, 38–52.
12. Kragh-Hansen, U. (1981). Molecular aspects of ligand binding to serum albumin. *Pharmacol. Rev.* **33**, 17–53.
13. Kragh-Hansen, U., Dørge, E. & Pedersen, A. O. (2005). Rate-of-dialysis technique: theoretical and practical aspects. *Anal. Biochem.* **340**, 145–153.
14. Kenyon, M. A. & Hamilton, J. A. (1994). ^{13}C NMR studies of the binding of medium-chain fatty acids to human serum albumin. *J. Lipid Res.* **35**, 458–467.
15. Kragh-Hansen, U. (1991). Octanoate binding to the indole- and benzodiazepine-binding region of human serum albumin. *Biochem. J.* **273**, 641–644.
16. Ashbrook, J. D., Spector, A. A. & Fletcher, J. E. (1972). Medium chain fatty acid binding to human plasma albumin. *J. Biol. Chem.* **247**, 7038–7042.
17. Honoré, B. & Brodersen, R. (1988). Detection of carrier heterogeneity by rate of ligand dialysis: medium-chain fatty acid interaction with human serum albumin and competition with chloride. *Anal. Biochem.* **171**, 55–66.
18. Goodman, D. S. (1958). The interaction of human serum albumin with long-chain fatty acid anions. *J. Am. Chem. Soc.* **80**, 3892–3898.
19. Peyre, V., Lair, V., André, V., le Maire, G., Kragh-Hansen, U., le Maire, M. & Møller, J. V. (2005). Detergent binding as a sensor of hydrophobicity and polar interactions in the binding cavities of proteins. *Langmuir*, **21**, 8865–8875.
20. Pedersen, A. O., Hust, B., Andersen, S., Nielsen, F. & Brodersen, R. (1986). Laurate binding to human serum albumin. Multiple binding equilibria investigated by a dialysis exchange method. *Eur. J. Biochem.* **154**, 545–552.
21. Ashbrook, J. D., Spector, A. A., Santos, E. C. & Fletcher, J. E. (1975). Long chain fatty acid binding to human plasma albumin. *J. Biol. Chem.* **250**, 2333–2338.
22. Oida, T. (1986). ^1H-NMR study on the interactions of

human serum albumin with free fatty acid. *J. Biochem.* **100**, 1533–1542.
23. Pedersen, A. O., Honoré, B. & Brodersen, R. (1990). Thermodynamic parameters for binding of fatty acids to human serum albumin. *Eur. J. Biochem.* **190**, 497–502.
24. Pedersen, A. O., Mensberg, K.-L. D. & Kragh-Hansen, U. (1995). Effects of ionic strength and pH on the binding of medium-chain fatty acids to human serum albumin. *Eur. J. Biochem.* **233**, 395–405.
25. Pedersen, A. O. & Brodersen, R. (1988). Myristic acid binding to human serum albumin investigated by dialytic exchange rate. *J. Biol. Chem.* **263**, 10236–10239.
26. Tanford, C. (1972). Hydrophobic free energy, micelle formation and the association of proteins with amphiphiles. *J. Mol. Biol.* **67**, 59–74.
27. Watanabe, H., Tanase, S., Nakajou, K., Maruyama, T., Kragh-Hansen, U. & Otagiri, M. (2000). Role of Arg-410 and Tyr-411 in human serum albumin for ligand binding and esterase-like activity. *Biochem. J.* **349**, 813–819.
28. Watanabe, H., Kragh-Hansen, U., Tanase, S., Nakajou, K., Mitarai, M., Iwao, Y. *et al.* (2001). Conformational stability and warfarin-binding properties of human serum albumin studied by recombinant mutants. *Biochem. J.* **357**, 269–274.
29. Nakajou, K., Watanabe, H., Kragh-Hansen, U., Maruyama, T. & Otagiri, M. (2003). The effect of glycation on the structure, function and biological fate of human serum albumin as revealed by recombinant mutants. *Biochim. Biophys. Acta*, **1623**, 88–97.
30. Fasano, M., Curry, S., Terreno, E., Galliano, M., Fanali, G., Narciso, P. *et al.* (2005). The extraordinary ligand binding properties of human serum albumin. *IUBMB Life*, **57**, 787–796.
31. Yamasaki, K., Maruyama, T., Yoshimoto, K., Tsutsumi, Y., Narazaki, R., Fukuhara, A. *et al.* (1999). Interactive binding to the two principal ligand binding sites of human serum albumin: effect of the neutral-to-base transition. *Biochim. Biophys. Acta*, **1432**, 313–323.
32. Simard, J. R., Zunszain, P. A., Ha, C.-E., Yang, J. S., Bhagavan, N. V., Petitpas, I. *et al.* (2005). Locating high-affinity fatty acid-binding sites on albumin by x-ray crystallography and NMR spectroscopy. *Proc. Natl Acad. Sci. USA*, **102**, 17958–17963.
33. Sjödin, T. (1977). Circular dichroism studies on the inhibiting effect of oleic acid on the binding of diazepam to human serum albumin. *Biochem. Pharmacol.* **26**, 2157–2161.
34. Cunningham, V. J., Hay, L. & Stoner, H. B. (1975). The binding of L-tryptophan to serum albumins in the presence of non-esterified fatty acids. *Biochem. J.* **146**, 653–658.
35. Koh, S.-W. M. & Means, G. E. (1979). Characterization of a small apolar anion binding site of human serum albumin. *Arch. Biochem. Biophys.* **192**, 73–79.
36. Simard, J., Zunszain, P. A., Hamilton, J. A. & Curry, S. (2006). Location of high and low affinity fatty acid binding sites on human serum albumin revealed by NMR drug-competition analysis. *J. Mol. Biol.* **361**, 336–351.
37. Kragh-Hansen, U., Pedersen, A. O., Galliano, M., Minchiotti, L., Brennan, S. O., Tárnoky, A. L. *et al.* (1996). High-affinity binding of laurate to naturally occurring mutants of human serum albumin and proalbumin. *Biochem. J.* **320**, 911–916.
38. Campagnoli, M., Kragh-Hansen, U., Pedersen, A. O., Amoresano, A., Lyon, A. W., Cesati, R. *et al.* (2003). Structural analysis, fatty acid and thyroxine binding properties of Vancouver and Naskapi variants of human serum albumin. *Clin. Biochem.* **36**, 597–605.
39. Chen, R. F. (1967). Removal of fatty acids from serum albumin by charcoal treatment. *J. Biol. Chem.* **242**, 173–181.

Edited by R. Huber

(Received 7 June 2006; received in revised form 17 July 2006; accepted 22 August 2006)
Available online 25 August 2006

Drug Metab. Pharmacokinet. 21 (2): 140–146 (2006).

Regular Article

The Structural and Pharmacokinetic Properties of Oxidized Human Serum Albumin, Advanced Oxidation Protein Products (AOPP)

Yasunori IWAO[1], Makoto ANRAKU[1], Mikako HIRAIKE[1], Keiichi KAWAI[2], Keisuke NAKAJOU[1], Toshiya KAI[3], Ayaka SUENAGA[1] and Masaki OTAGIRI[1,*]

[1]*Department of Biopharmaceutics, Graduate School of Pharmaceutical Sciences, Kumamoto University, Kumamoto, Japan*
[2]*School of Health Sciences, Faculty of Medicine, Kanazawa University, Ishikawa, Japan*
[3]*Pharmaceutical Research Center, Nipro Corporation, Kusatsu, Shiga, Japan*

Full text of this paper is available at http://www.jstage.jst.go.jp/browse/dmpk

Summary: To determine the pharmacokinetic properties of advanced oxidation protein products (AOPP), we prepared oxidized human serum albumin (oxi-HSA) using chloramine-T (a hypochlorite analogue) *in vitro*. The AOPP and dityrosine content of oxi-HSA (AOPP content, 244.3 ± 12.3 μM; dityrosine content, 0.7 ± 0.11 nmol of dityrosine/mg protein) were similar to those of uremic patients. In structural analysis, the increases in AOPP and dityrosine content of HSA induced slight decreases in its α-helical content. In pharmacokinetic analysis, oxi-HSA left the circulation rapidly, and organ distribution of oxi-HSA 30 min after intravenous injection was 51% for the liver, 23% for the spleen, and 9% for the kidney, suggesting that the liver and spleen were the main routes of plasma clearance of oxi-HSA. The liver and spleen uptake clearance of oxi-HSA were significantly greater than those of normal HSA (CLliver, 5058 ± 341.6 vs 24 ± 4.2 μL/hr [$p < 0.01$]; CLspleen, 2118 ± 322.1 vs 32 ± 2.7 μL/hr [$p < 0.01$]). However, uptake by other organs was not significantly affected by oxidation. These results suggest that the liver and spleen play important roles in elimination of AOPP.

Key words: human serum albumin; structural change; advanced oxidation protein products; pharmacokinetics

Introduction

Recent evidence indicates that oxidative stress plays an important role in the pathogenesis of chronic renal failure (CRF).[1] Oxidative stress is defined as increased production of reactive oxygen species (ROS) due to an imbalance of oxidant/antioxidant systems. Activated phagocytes are a major source of ROS, and play a fundamental role in host defense.[2] Neutrophils contain the heme enzyme myeloperoxidase (MPO), which catalyzes the reaction of chloride ion with hydrogen peroxide (H_2O_2), to generate the large amounts of hypochlorous acid (HOCl) produced by neutrophils.[3] HOCl-modified proteins have been detected in atherosclerotic lesions[4] and plasma from glomerular nephritis patients.[5] To estimate the degree of oxidant-mediated protein damage in plasma of CRF patients, researchers have assayed levels of advanced oxidation protein products (AOPP) in CRF plasma. Witko-Sarsat *et al.* showed that *in vivo* levels of AOPP strongly correlate with creatinine clearance, indicating that AOPP are excellent markers of progression of CRF.[6] HOCl-treated HSA and *in vivo*-generated AOPP can trigger oxidative bursts in neutrophils and monocytes *in vitro*, indicating that they both can act as true inflammatory mediators.[7] Results of *in vitro* studies of mechanisms of AOPP production indicate that HOCl-treated HSA can trigger an oxidative burst.[7] However, the mechanisms by which AOPP are degraded and eliminated from circulating blood remain unclear.

Recently, there have been reports of several types of receptors that bind to modified albumin, including SR-A (human scavenger receptor class A, which binds LDL)[8,9] and CD36 (scavenger receptor class B family).[10,11] Despite such important findings, it remains unclear whether physiologically oxidized HSA (oxi-

Received; October 14, 2005, Accepted; November 25, 2005
**To whom correspondence should be addressed*: Prof. Masaki OTAGIRI, Ph.D., *Department of Biopharmaceutics, Graduate School of Pharmaceutical Sciences, Kumamoto University, 5-1 Oe-honmachi, Kumamoto 862-0973, Japan. Tel. +81-96-371-4150, Fax. +81-96-362-7690, E-mail: otagirim@gpo.kumamoto-u.ac.jp*

HSA) containing AOPP behaves in the same way as other modified albumins.

In the present study, using normal HSA and chloramine-T-treated HSA (oxi-HSA), we examined the mechanisms by which AOPP are degraded and eliminated from circulating blood.

Material and Methods

Materials and animals: Chloramine-T (CT) was purchased from Nacalai Tesque, Inc. (Kyoto, Japan). The fluorescence probe 1, 1-bis-4-anilino-naphthalene-5,5-sulfonic acid (bis-ANS) was purchased from Sigma (St Louis, MO, USA). $^{111}InCl_3$ (74 MBq/mL in 0.02 N HCl) was donated by Nihon Medi-Physics (Takarazuka, Japan). All chemicals used were of the highest grade commercially available, and all solutions were prepared using deionized, distilled water. Male ddY mice (24–26 g) were purchased from the Shizuoka Agricultural Cooperative Association for Laboratory Animals (Shizuoka, Japan). Animals were maintained under conventional housing conditions. All animal experiments were conducted in accordance with the principles and procedures outlined in the National Institute of Health Guide for the Care and Use of Laboratory Animals.

Preparation of oxi-HSA: HSA (300 μM) was incubated for 1 h at 37°C in an oxygen-saturated solution containing 100 mM CT in phosphate buffer (pH 8.0). After incubation, the oxidation reaction was stopped by extensive dialysis of the solution against water. As a negative control, albumin was incubated in buffer alone. The oxi-HSA and negative control HSA were stored at −20°C until used.

Western blot analysis: Oxi-HSA was detected by performing Western blot analysis. The antibodies used were an anti-HSA primary antibody raised in a rabbit and an anti-rabbit secondary antibody conjugated to horseradish peroxidase.

Determination of AOPP and dityrosine content: AOPP content of oxi-HSA was determined using a previously reported semi-automated method.[6] Dityrosine content was assayed by measuring fluorescence after the sample was diluted to 2 μM. Fluorescence emission spectra of dityrosine were recorded at 410 nm after excitation at 325 nm, using a spectrofluorometer (FP-6200 Jasco) as described previously.[12]

Amino acid analysis: The amino acid composition of oxi-HSA was quantified by performing amino acid analysis after acid hydrolysis with 6 M HCl for 24 h at 110°C, using an amino acid analyzer (L-8500A, Hitachi, Tokyo, Japan) as described previously.[13]

Structural properties of oxi-HSA: CD spectra were obtained using a JASCO J-720 spectropolarimeter (JASCO, Tokyo, Japan) at 25°C. The effective hydrophobicity of oxi-HSA was estimated using the fluorescent characteristics of bis-ANS (10 μM) at 25°C. Each compound was excited at 394 nm, and fluorescence spectra were recorded on a Jasco FP-770 fluorescence spectrometer (Tokyo, Japan).

***In Vivo* Experiments:** All proteins were radiolabeled with ^{111}In using the bifunctional chelating reagent DTPA anhydride, according to the method of Hnatowich *et al.*.[14,15] Mice received tail vein injections of ^{111}In-labeled proteins in saline, at a dose of 1 mg/kg, and were housed in metabolic cages to allow the collection of urine samples. At appropriate intervals after the injection, blood was collected from the vena cava under ether anesthesia, and plasma was obtained by centrifugation. The liver, kidney, spleen, lung, heart and muscle were excised, rinsed with saline and weighed. The radioactivity of each sample was measured using a well-type NaI scintillation counter (ARC-500, Aloka, Tokyo). Pharmacokinetic analyses were performed as follows. The plasma ^{111}In radioactivity concentrations were normalized with respect to the percentage of the dose per mL, and were analyzed using the nonlinear least-square program MULTI.[16] Tissue distribution was evaluated using the organs uptake clearance method (CLorgans), as described previously.[17]

Cellular assays: Endocytic uptake was determined as described previously.[18,27] RAW 264.7 cells were seeded in each well of a 24-well culture plate in 1.0 mL RPMI 1640 medium, containing 10% FCS, 100 U/mL penicillin, and 100 μg/mL streptomycin, and cultured for 12 hr to subconfluence. The cells were washed with 1.0 mL PBS and replaced with Dulbecco's modified Eagle's medium containing 3% BSA, 100 U/mL penicillin, and 100 μg/mL streptomycin (medium A). The cells in each well were incubated at 37°C for 6 hr in 0.5 mL medium A with various concentrations of ^{125}I-control- or oxi-HSA in the presence (non-specific) or absence (total) of 50-fold unlabeled each ligands. At the indicated time, 0.375 mL of the culture medium was taken from each well and mixed with 0.15 mL 40% trichloroacetic acid (TCA) in a vortex mixer. We added 0.1 mL of 0.7 mol/L $AgNO_3$ to this solution, which was followed by centrifugation. The resulting supernatant (0.25 mL) was used to determine TCA-soluble radioactivity, which was taken as an index of cellular degradation, since proteins are endocytosed by the cells and delivered to lysosomes where they are degraded and excreted into the culture medium in a TCA-soluble form. Then, each well was washed three times with 1.0 mL ice-cold PBS. The cells were lysed with 1.0 mL of 0.1 N NaOH for 1 hr at 37°C to determine the cell-associated radioactivity. Specific cell-association or degradation were determined by subtracting non-specific from total.

Statistics: Statistical analyses were performed using

Student's t-test.

Results

Western blot analysis of oxi-HSA: After exposure to CT, protein aggregation or cross-linking was clearly indicated by the presence of a smear in the high molecular weight range. The high-molecular-weight fragments were recognized by the anti-HSA antibody (**Fig. 1**). These results suggest that treatment of HSA with CT causes aggregation and cross-linking due to oxidation (oxi-HSA).

The characteristics of oxi-HSA: The AOPP content of oxi-HSA was significantly greater than that of control-HSA (244.3 ± 12.3 vs 10.3 ± 6.3 μM; $p<0.01$; **Table 1**). Dityrosine content of oxi-HSA was also significantly greater than that of control-HSA (0.7 ± 0.11 vs 0.32 ± 0.13 nmol dityrosine per mg protein; $p<0.01$). These characteristics of oxi-HSA are similar to those of proteins in uremic plasma (**Table 1**). The results of amino acid analysis indicate that oxidation of HSA induced significant changes in its content of certain amino acid residues including tyrosine and basic amino acids (**Table 2**).

Structural properties of oxi-HSA: To obtain information about protein structure, CD measurements were performed in the far-UV regions (**Fig. 2A**). The molar ellipticity of oxi-HSA was significantly less than that of control-HSA in the far-UV CD spectrum. The effects of oxidation on the structural properties were examined using the fluorescence probe bis-ANS. The spectra indicate that oxidation of HSA causes a decrease in its accessible hydrophobic areas (**Fig. 2B**). These results suggest that the structure of HSA is significantly changed by oxidation.

Pharmacokinetic properties of oxi-HSA: **Figure 3A** shows the time courses for radioactivity of ^{111}In-labeled preparations of oxi-HSA. Oxi-HSA had a shorter half-life than control-HSA. To determine the reasons for the decreased plasma half-life of oxi-HSA, we examined organ uptake. Liver, spleen and kidney uptake of oxi-HSA increased with time, and were all much greater than those of control-HSA (**Fig. 3B-D**, **Table 3**). Uptake by other organs was not significantly affected by oxidation (data not shown).

Discussion

Although *in vivo* studies indicate that the constant plasma half-life of radioisotope-labeled native albumin is 2 to 2.5 days in rats,[19] modified albumin has been

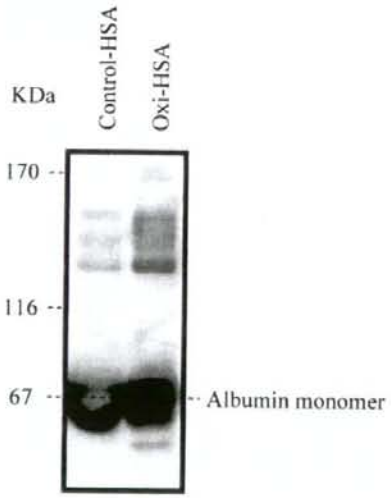

Fig. 1. Western blot analysis of control-HSA and oxi-HSA.

Table 2. Changes in amino acids composition of oxi-HSA.

Amino acids	Literature value	Control-HSA (n = 3)	Oxi-HSA (n = 3)
Thr	28	22.5 ± 0.3	22.4 ± 0.4
Ser	24	24.5 ± 0.2	24.6 ± 0.3
Gly	12	12.0 ± 0.3	12.8 ± 0.3
Ala	62	62.0 ± 0.4	62.0 ± 0.1
Val	41	38.6 ± 0.2	39.4 ± 0.4
Met	6	3.2 ± 0.1	2.14 ± 0.2
Ile	8	7.7 ± 0.5	7.8 ± 0.1
Leu	61	61.3 ± 0.4	61.8 ± 0.1
Tyr	18	16.0 ± 0.3	6.7 ± 0.4*
Lys	59	53.0 ± 0.1	26.9 ± 0.4*
His	16	15.1 ± 0.4	14.5 ± 0.4
Arg	24	23.9 ± 0.4	18.6 ± 0.3*

*Significantly different ($P<0.01$) from control-HSA. Data are mean ± SD.

Table 1. AOPP and dityrosine content of HSA treated with chloramine T.

	Control-HSA	Oxi-HSA	Normal subjects	HD patients
AOPP (μM)	10.3 ± 6.3	244.3 ± 12.3*	33.9 ± 3.4[a]	267.5 ± 16.5[a]
Dityrosine (nmol/mg protein)	0.32 ± 0.13	0.7 ± 0.11*	0.36 ± 0.05[a]	1.03 ± 0.12[a]

*Significantly different ($P<0.01$) from control-HSA. Data are mean ± SD.
[a]Ref. 6.